S-acylation regulates the trafficking and stability of the unconventional Q-SNARE STX19

Authors: Khamal K. Ampah[1,5], Jennifer Greaves[2], Amber S. M. Shun-Shion[1], Asral W. B. A. Asnawi[1,7], Jessica A. Lidster[1,6], Luke H. Chamberlain[3], Mark O. Collins[1, 4] and Andrew A. Peden[1]

[1]Department of Biomedical Science, Centre for Membrane Interactions and Dynamics, University of Sheffield, Firth Court, Sheffield, S10 2TN, United Kingdom

[2]Faculty of Health and Life Sciences, Coventry University, Science and Health Building, 20 Whitefriars Street, Coventry CV1 2DS, United Kingdom

[3]Strathclyde Institute of Pharmacy and Biomedical Sciences, University of Strathclyde, Glasgow G4 0RE, United Kingdom

[43]Faculty of Science, Mass Spectrometry Centre, University of Sheffield, Brook Hill Road, Sheffield, S3 7HF, United Kingdom

[5]Current address: London School of Hygiene and Tropical Medicine, Keppel Street, London, WC1E 7HT, United Kingdom

[6]Current address: University of Leeds, Leeds, LS2 9JT, United Kingdom

[7]Faculty of Medicine and Health Sciences, University Sains Islam Malaysia, 55700 Kuala Lumpur, Malaysia

Corresponding author: A. Peden

Email: a.peden@sheffield.ac.uk

Phone: 0114-222-2312

SUMMARY

The Q-SNARE STX19 is S-acylated by Golgi localised S-acyltransferases and this lipidation targets the protein to MICAL-L1-positive tubular recycling endosomes and also protects it from proteasomal degradation.

ABSTRACT

STX19 is an unusual Q_a-SNARE as it lacks a C-terminal transmembrane domain. However, it is efficiently targeted to post-Golgi membranes. We have set out to determine the intracellular localisation of endogenous STX19 and elucidate the mechanism by which it is targeted to membranes. We have found that a pool of STX19 is localised to tubular recycling endosomes where it co-localises with MICAL-L1 and Rab8. Using a combination of genetic, biochemical and cell based approaches we have identified that STX19 is S-acylated at its C-terminus and is a substrate for several Golgi localised S-acyltransferases, suggesting that STX19 is initially S-acylated at the Golgi before trafficking to the plasma membrane and endosomes. Surprisingly, we have found that S-acylation is a key determinant in targeting STX19 to tubular recycling endosomes, suggesting that S-acylation may play a general role in directing proteins to this compartment. In addition, S-acylation also protects STX19 from proteosomal degradation indicating that S-acylation regulates the function of STX19 at multiple levels.

INTRODUCTION

Over the past 30 years, the majority of the molecular machinery required for intracellular protein transport has been identified and functionally characterised. However, our understanding of how this machinery is regulated by post-translational modifications is less clear. This is especially true for lipid-based modifications which are generally more difficult to study. It is estimated that up to 10% of the human proteome may be S-acylated (Blanc et al., 2015) and the number of confirmed S-acylated proteins is increasing rapidly due to proteomic based approaches (Collins et al., 2017; Martin and Cravatt, 2009; Martin et al.,

2011). However, for the majority of these proteins, it is unclear what role S-acylation plays in regulating their function. S-acylation is a reversible post-translational modification of free cysteine residues with fatty acids, predominantly palmitic acid (Smotrys and Linder, 2004); hence the process is also referred to as palmitoylation. However, other fatty acids with different chain lengths and unsaturation can also be added to S-acylated proteins (Muszbek et al., 1999). S-acylation not only targets peripheral proteins to membranes but also regulates protein trafficking, turnover and cell signalling (Akimzhanov and Boehning, 2015; Linder and Deschenes, 2007; Misaki et al., 2010; Schmick et al., 2014).

S-acylation, in humans, is catalysed by a family of 23 S-acyltransferases (Fukata et al., 2004). These enzymes are multi-spanning transmembrane proteins that are localised to a broad range of intracellular membranes including the ER, Golgi, and plasma membrane (Greaves and Chamberlain, 2011a; Ohno et al., 2006). All S-acyltransferases (also known as zDHHC enzymes) have a highly conserved zinc finger like domain that contains the amino acid sequence DHHC (Asp-His-His-Cys) which is essential for their activity. On the whole, it is not well understood how these enzymes recognise their substrates, so the extent of substrate specificity remains unclear. S-acylation is the only lipid-based modification that is reversible and there are several examples where a cycle of S-acylation and de-S-acylation is critical for regulating trafficking and signalling (Akimzhanov and Boehning, 2015; Schmick et al., 2014). Two serine hydrolases, APT1 and APT2 were initially thought to be the only enzymes that catalyse de-S-acylation in the cytoplasm (Duncan and Gilman, 1998; Tomatis et al., 2010). However, there is increasing evidence there may be many more serine hydrolases involved in this process (Lin and Conibear, 2015; Martin et al., 2011; Yokoi et al., 2016).

Intracellular membrane fusion is driven by a family of evolutionarily conserved proteins known as SNAREs (Jahn and Scheller, 2006). The majority of SNAREs (32 out of 38) have a transmembrane domain at their C-termini which, targets them to membranes (Bock et al., 2001; Kloepper et al., 2007). However, there are several SNAREs that lack a membrane-spanning sequence. These include the R-SNARE, Ykt6; the Q_a-SNAREs, syntaxin 11 (STX11) and syntaxin 19 (STX19); the Q_{bc}-SNAREs SNAP23, 25, 29 and 47. Most of these SNAREs are targeted to membranes via the post-translational lipidation of conserved cysteine residues. For example, Ykt6 is both farnesylated and S-acylated (Fukasawa et al., 2004). SNAP23 and SNAP25 are S-acylated at a cysteine-rich domain located just downstream of the first SNARE

motif (Greaves et al., 2010) and STX11 is S-acylated at its C-terminus (Hellewell et al., 2014). There is significant evidence that the lipidation of these SNAREs not only regulates their membrane targeting but also regulates their trafficking and function. For example, S-acylation of Ykt6 at cysteine 194 leads to a conformational switch that exposes the SNARE motif and makes it accessible for interaction with other SNAREs (Fukasawa et al., 2004; Gordon et al., 2017; Wen et al., 2010). Altering the levels of SNAP25 S-acylation by mutating key cysteine residues changes its localisation suggesting that S-acylation can regulate SNAP25 trafficking (Greaves and Chamberlain, 2011b). S-acylation is also required for the correct targeting of STX11 to the immune synapse (Hellewell et al., 2014), where STX11 is thought to play a role in the regulation of lytic granule fusion with the plasma membrane (D'Orlando et al., 2013). Loss of STX11 function in humans causes the immunoproliferative disorder FHL4 (zur Stadt et al., 2005). Several mutations that cause this disorder result in the truncation of the cysteine-rich domain of STX11 (Hellewell et al., 2014), highlighting the importance of S-acylation for STX11 function.

STX19 is a close homologue of STX11 (38% amino acid identity) (Wang et al., 2006) and has been identified as an S-acylated protein in a global proteomics screen (Kang et al., 2008). However, it is unclear which residues in STX19 are S-acylated and what role S-acylation has in regulating STX19 trafficking and function. Like STX11, STX19 has a restricted tissue distribution and its mRNA is predominantly detected in mucosal epithelium of the gut and the skin (Wang et al., 2006). Work from our group and others have shown that depletion of STX19 using siRNA perturbs the constitutive secretion of both soluble and transmembrane anchored cargo (Gordon et al., 2010) (Simpson et al., 2012). Immunoprecipitation studies have found that STX19 interacts with post-Golgi SNAREs thought to be involved in fusion with the cell surface, suggesting that STX19 may be a novel plasma membrane localised Q-SNARE involved in biosynthetic transport (Gordon et al., 2010).

In this study, we sought to gain an insight into the function of STX19 by elucidating where STX19 is localised within the cell and determining how S-acylation regulates its trafficking. We have found that the highly conserved cysteine-rich domain of STX19 (KKRNPCRVLCCWCCPCCSSK) is S-acylated at several cysteines and is necessary and sufficient for targeting STX19 to tubular recycling endosomes and the plasma membrane. Blocking S-acylation by either treating cells with the 2-bromopalmitate or mutating cysteine residues in

the cysteine-rich domain alters the steady-state localisation of STX19. In addition, these perturbations reduce expression levels of STX19 suggesting that S-acylation regulates STX19 stability. The S-acylation of STX19 can be catalysed by several Golgi localised zDHHCs suggesting that STX19 is first S-acylated at the Golgi and subsequently traffics to the cell surface and tubular recycling endosomes. Over expression of GFP tagged STX19 perturbs the trafficking of Rab8 suggesting that STX19 may be involved in the fusion of Rab8 positive vesicles with the plasma membrane.

EXPERIMENTAL PROCEDURES

Antibodies and Reagents

The polyclonal antibody against STX19 was generated by immunising rabbits with GST-STX19[1-100]. The antiserum was affinity purified as in (Page and Robinson, 1995) and diluted 1/200 for microscopy. An anti-HA mouse monoclonal antibody (16B12) was purchased from BioLegend (Cat No 901503; 1/200 microscopy and 1/1000 blotting). A rabbit polyclonal and monoclonal antibody to Rab8A were purchased from ProteinTech (Cat No 55296-1-AP; 1/200 microscopy) and Cell Signalling Technology, respectively (Cat No Rabbit mAb #6975; 1/500 for microscopy). The rabbit polyclonal antibody against GFP (1/200 microscopy and 1/1000 blotting) was previously described (Gordon et al., 2017). The Alexa-488 and 594 conjugated secondary antibodies for fluorescence microscopy were purchased from ThermoFisher and used at 1/1000. The HRP conjugated secondary antibodies for immunoblotting were purchased from Jackson ImmunoResearch Laboratories and used at 1/5000. For click chemistry analysis, mouse anti-GFP antibody (JL8) was obtained from TaKaRa Clontech (Cat No 632381, 1/1000 blotting); rat anti-HA antibody (3F10) was purchased from Sigma (Cat No 000000011867423001, 1/1000 blotting) and the IR dye conjugated secondary antibodies were purchased from LI-COR. All restriction enzymes were purchased from New England Biolabs. All primers were purchased from SigmaAldrich. GFP-Trap beads were purchased from Chromotek (Cat No gta-20).

Expression constructs

Human STX19 (Gene ID: 415117) was used as the template for all the constructs used in this study. Wild-type and mutant HA-STX19 expression constructs were generated by PCR and cloned into pIRES-NEO (GenBank Accession number: U89673). GFP-STX19 expression constructs (GFP-STX19[1-294] and GFP-STX19[1-277]) were generated by PCR and cloned into pEGFP-C1 (GenBank Accession number: U55763). The GFP-cysteine-rich domain construct (GFP-STX19[275-294]) was generated by annealing oligos and ligating them into pEGFP-C3 (GenBank Accession number: U57607). FKBP-STX19[1-294] and FKBP-STX19[1-277] were generated by PCR and cloned into pIRES-NEO. The HA tagged zDHHC expression library was a kind gift from M. Fukata (17). The pCAG-mGFP (GFP fused with GAP43 S-acylation sequence) was obtained from Addgene (14757) (Matsuda and Cepko, 2007). The GFP-HRAS construct was a kind gift from I. Prior (University of Liverpool). The MitoTRAP (pMito-mCherry-FRB) and GFP-FKBP constructs were a generous gift from S. Royle (Cheeseman et al., 2013). All constructs were sequenced using the University of Sheffield's Core Genomic Facility.

Cell culture and transfections

HeLaM cells were originally obtained from the laboratory of M.S Robinson (University of Cambridge) and HEK-293T (CRL-3216) cells were obtained from ATCC. Both cell lines were routinely tested for mycoplasma contamination. HeLaM and HEK-293T cells were grown in DMEM supplemented with 10% fetal bovine serum (Life technologies), 100 IU/mL penicillin, 100 μg/mL streptomycin and 2 mM glutamine (Sigma-Aldrich) at 37°C in a 5% CO_2 humidified incubator. In some instances, HeLaM cells were treated with either 5 μM MG132 (Cayman Chemical, USA) or 100 μM 2-bromopalmitate (Sigma-Aldrich). HeLaM and HEK-293 cells were transfected using PEI (ratio 1 part DNA to 5 parts PEI). Cells were analysed 24-48 hours post-transfection. siRNA transfections were performed as in Gordon et al., 2010.

Immunofluorescence microscopy

Approximately, 2×10^5 HeLaM cells were seeded onto glass coverslips and grown overnight. The cells were rapidly fixed, by adding an equal volume of room temperature (RT) 4% paraformaldehyde in PBS to the culture media, as soon as the cells were removed from the incubator. After one minute, the fixative was removed and replaced with fresh fixative. The cells were incubated for a further 15 minutes at RT. The fixative was removed and the cells washed three times with PBS. The cells were incubated for 5 minutes with 0.1 M glycine in PBS. The cells were permeabilised using 0.1% saponin in PBS containing 5% FCS. The cells were stained with the appropriate primary and secondary antibodies for one hour at RT. The coverslips were mounted onto microscope slides using ProLong Gold antifade reagent (ThermoFisher) and observed with a 60X oil immersion objective (Olympus BX61 motorised wide field epifluorescence microscope). Images were captured using a Hamamatsu Orca monochrome camera and processed using ImageJ.

Immunoprecipitation acyl-release assay

Cells expressing GFP-STX19$^{275-294}$ were harvested 48 hours post-transfection by scraping and centrifugation (1000 rpm for 5 minutes at 4°C). The cell pellets were resuspended in 1 mL of RIPA lysis buffer, (50 mM Tris (pH 7.4), 150 mM NaCl, 1 mM EDTA (pH 8.0), 1% NP-40, 0.5% Sodium deoxycholate, 0.1% SDS, and protease inhibitors) and passed through a QIAShredder (Qiagen). The samples were then incubated for one hour at 4°C to ensure complete solubilisation. Insoluble material was removed by centrifugation at 13,000 rpm for 15 minutes at 4°C. The supernatant was then incubated with GFP-Trap beads for 3 hours at 4°C (Rothbauer et al., 2008). The beads were washed three times with RIPA buffer and two times with Tris buffered saline. The immunoisolated protein was then reduced and alkylated using 5 mM TCEP and 50 mM iodoacetamide in 50 mM Tris (pH 8). The beads were then washed five times with 50 mM Tris (pH 7.5). The beads were then divided in to two samples. Sample (a) was incubated with 1 M hydroxylamine in 50 mM Tris (pH 7.5), to cleave thioester bonds and sample (b) was incubated with 50 mM Tris (pH 7.5) as a control. The beads were washed three times with 50 mM Tris (pH 7.5). The protein was eluted from

the beads using 8 M Guanidine-HCl at 95 °C for 10 minutes. The eluted protein was digested for 4 hours at 37 °C with 0.5 µg of trypsin prepared in 100 mM ammonium bicarbonate solution (pH 8). The peptides were dried overnight using a vacuum concentrator. Peptides were resuspended in 0.5 % formic acid for 10 minutes at RT with agitation.

Mass spectrometry analysis

Peptides were analysed by nanoLC-MS/MS on an Orbitrap Elite (ThermoFisher) hybrid mass spectrometer equipped with a nanospray source, coupled with an Ultimate RSLCnano LC System (Dionex). The system was controlled by Xcalibur 2.1 (ThermoFisher) and DCMSLink 2.08 (Dionex). Peptides were desalted on-line using a micro-Precolumn cartridge (C18 Pepmap 100, LC Packings) and then separated using a 60 min RP gradient (4-32% acetonitrile/0.1% formic acid) on an EASY-Spray column, 15 cm x 50 µm ID, PepMap C18, 2 µm particles, 100 Å pore size (Thermo). The mass spectrometer was operated with a cycle of one MS (in the Orbitrap) acquired at a resolution of 60,000 at m/z 400, with the top 20 most abundant multiply-charged (2+ and higher) ions in a given chromatographic window subjected to CID fragmentation in the linear ion trap. An FTMS target values of 1e6 and an ion trap MSn target value of 1e4 was used and with the lock mass (445.120025) enabled. Maximum FTMS scan accumulation time of 500ms and maximum ion trap MSn scan accumulation time of 100ms were used. Dynamic exclusion was enabled with a repeat duration of 45s with an exclusion list of 500 and exclusion duration of 30s. MS data was analysed using MaxQuant (Cox and Mann, 2008) version 1.5.5.1. Data were searched against human UniProt sequence databases (downloaded June 2015) using the following search parameters: trypsin with a maximum of 2 missed cleavages, 7 ppm for MS mass tolerance, 0.5 Da for MS/MS mass tolerance, with Acetyl (Protein N-term) and Oxidation (M) set as variable modifications and carbamidomethyl (C) as a fixed modification. Previously S-acylated sites were identified by the lack of carbamidomethyl (C) (-57.0214) which was set as a variable modification. A maximum of 6 modifications per peptide was allowed. A protein FDR of 0.01 and a peptide FDR of 0.01 was used for identification level cut offs. Label free quantification of peptides +/- hydroxylamine treatment was performed using MaxQuant calculated peptide intensities. S-acylation site occupancies were calculated by expressing peptide intensities of modified peptides to their unmodified counterparts.

Immunoblotting

Cells were washed three times with ice-cold PBS and lysed with SDS sample buffer containing 5% β-mercaptoethanol. The cell lysates were passed through a QIAShredder (Qiagen) three times to sheer chromosomal DNA. The lysates were boiled at 100˚C for 10 minutes. The samples were then separated using SDS-PAGE and transferred overnight onto a 0.45 μm PVDF membrane (GE Healthcare Life Sciences). The membranes were blocked in PBS containing 5% milk powder and 1% Tween-20 at RT for 30 minutes. The membranes were probed with specific antibodies diluted in the blocking buffer. The probed membranes were washed thoroughly with PBS and the damp membranes incubated with Clarity ECL Western blot Substrate for 5 minutes at RT. The excess substrate was removed and the signal detected using either X-ray film (Fujifilm) or a LiCOR c-DiGiT. Quantification of the immunoblots was performed using Image Studio Lite Ver 4.0 (Li-COR Inc.).

17-octadecynoic acid labelling coupled to click chemistry

The 17-octadecynoic acid labelling coupled to click chemistry was performed as described in (Martin and Cravatt, 2009; Yap et al., 2010) with some minor modifications. HEK-293T cells were seeded onto 24-well plates, grown overnight and co-transfected with 23 HA-tagged S-acyltransferases and GFP-STX19$^{1-294}$ or GFP-STX19$^{275-294}$ (0.8μg of STX19 construct to 1.6μg of HA-zDHHC). 24 hours post-transfection, the cells were serum-starved in DMEM containing 1 mg/ml fatty-acid free BSA for 30 minutes at 37°C. The cells were then labelled for 3 hours at 37ºC with 100 μM 17-octadecynoic acid. The cells were washed two times with ice-cold PBS and then lysed on ice in 50 mM Tris (pH8.0) containing 0.5% SDS and protease inhibitors. The cell lysates were then incubated with the click reaction buffer (final concentration; 2.5 μM IR-800 dye, 2 mM CuSO$_4$, 0.2 mM TBTA and 4 mM Ascorbic Acid). The click reaction buffer and ascorbic acid were freshly prepared on the day of the experiment. The samples were vortexed and incubated for 1 hour at RT with end-over-end rotation. After the click reaction, the proteins were precipitated using acetone and the pellets allowed to air-dry for 5 minutes. The pellets were resuspended in 1XSDS sample buffer containing 25mM DTT and heated at 95ºC for 5 minutes. The samples were separated

by SDS-PAGE (12%) and transferred on to nitrocellulose membranes and probed with antibodies against GFP and HA.

Statistical analysis

All bar graphs presented in this manuscript were prepared using GraphPad Prism (GraphPad Software). For each experiment, a minimum of three biological repeats were performed. In all graphs the error bars show the mean ± standard error mean. An unpaired t-test was performed using GraphPad Prism to calculate P values.

RESULTS

A pool of STX19 is localised to the plasma membrane and tubular recycling endosomes

To gain insight into the localisation of STX19 and its potential function we have transiently transfected HA-tagged STX19 into HeLaM cells (**Fig. 1A**). As previously reported, we observed recombinant STX19 at the plasma membrane and on intracellular membranes (Gordon et al., 2010; Wang et al., 2006). The intracellular labelling was very striking with STX19 present on branched tubular structures that were between 2-20μm in length, which emanate from the perinuclear region of the cell. A similar localisation pattern was also observed with a C-terminally tagged construct indicating that the position of the tag was not interfering with STX19 targeting (**Fig. 1A**). To determine if endogenous STX19 is also localised to branched tubular membranes we generated a rabbit polyclonal antibody to STX19 and performed immunostaining. Like recombinant STX19, we observed a pool of endogenous STX19 localised to branched tubular structures. The tubular staining is specific as the signal can be depleted using a previously validated siRNA targeting STX19 (**Fig. 1B**) (Gordon et al., 2010).

Endocytic recycling machinery such as Rab8 and MICAL-L1 are localised to tubular recycling endosomes (Rahajeng et al., 2012; Sharma et al., 2009). These endosomes contain endocytosed proteins such as MHC-I and GPI anchored proteins (CD55 and CD59). Thus, we hypothesised that STX19 may also be localised to this compartment. To determine if this is the case, we performed co-localisation experiments with endogenous STX19, MICAL-L1,

CD55 and recombinant Rab8 (**Fig. 1C**). As previously reported, MICAL-L1 and Rab8 were found on branched tubular membranes in the majority of cells. As predicted, these structures co-localise with endogenous STX19. CD55 is predominantly found at the cell surface in HelaM cells. However, a small intracellular pool can be observed that co-localises with STX19. Taken together, our results indicate that a pool of endogenous STX19 is found on tubular recycling endosomes.

The cysteine-rich domain of STX19 is required for targeting STX19 to the plasma membrane and tubular recycling endosomes

STX19 is a Q_a-SNARE that is predicted to have a folded H_{abc} domain and a single SNARE motif. Unlike the majority of Q_a–SNAREs, STX19 lacks the standard hydrophobic stretch of amino acids at its C-terminus that act as a membrane anchor. However, STX19 has a highly conserved cysteine-rich region at its C-terminus that has previously been predicted to be lipid modified (**Fig. 2A, Table S1**) (Wang et al., 2006). The conserved region consists of an upstream basic patch (K/R) followed by a series of cysteine residues separated by a bulky hydrophobic residue (W/F) and a proline residue. To investigate the importance of the cysteine-rich region in STX19 trafficking we have deleted this region and determined the localisation of the mutant protein. In addition, we also investigated the role of the SNARE motif in STX19 trafficking by deleting this region. Wild-type STX19 (STX19[1-294]) was localised to the plasma membrane and Rab8 positive tubules, whereas the mutant construct lacking the cysteine-rich domain (STX19[1-277]) was found in the cytoplasm (**Fig. 2B and quantified in C**), see **Fig. S1** for representative images showing Rab8 co-staining. In addition to the observed mis-localisation, we also observed a significant reduction in the levels of the STX19[1-277] construct so longer exposure times were required to obtain comparable images for this mutant construct (this phenotype is explored further further in **Fig. 6**). These results suggest that the cysteine-rich domain of STX19 is required for targeting the protein to the plasma membrane and Rab8 positive tubular recycling endosomes. Deletion of the coiled-coil domain from STX19 (STX19[Δ218-271]) did not significantly alter the localisation of STX19 suggesting that this domain is dispensable for its correct intracellular localisation (**Fig. 2B and quantified in C**).

To determine if the cysteine-rich region of STX19 is preferentially targeting STX19 to tubular recycling endosomes, we replaced it with the transmembrane domain of the endosomal Q_a-SNARE STX13 (Prekeris et al., 2000). HeLaM cells were transfected with the hybrid construct (STX19$^{1-277}$/STX13$^{251-276}$) and the localisation of the protein determined. The hybrid construct was effectively targeted to the plasma membrane but its association with the Rab8 positive tubules was significantly reduced suggesting that the cysteine-rich region provides trafficking information which allows STX19 to be targeted to tubular recycling endosomes (**Fig. 2B and quantified in C**). To explore this observation further, we fused the cysteine-rich region onto GFP. HeLaM cells were transfected with either full length STX19 (GFP-STX19$^{1-294)}$ or the cysteine-rich region alone (GFP-STX19$^{275-294}$). Both constructs were found at the plasma membrane and on tubular recycling endosomes as defined by co-localisation with Rab8 (**Fig. 2D**). Taken together, these results indicate that the cysteine-rich region of STX19 is capable of targeting proteins to tubular recycling endosomes without the need for any additional sorting information. Interestingly, other S-acylated proteins, such as RAS, are also trafficked to tubular recycling endosomes in HeLaM cells suggesting that S-acylation may have a more general role in targeting proteins to this compartment (**Fig. S2**).

Inhibition of S-acylation blocks the targeting of STX19 to the plasma membrane and tubular recycling endosomes

Our transfection studies indicated that the cysteine-rich domain of STX19 is able to target to membranes independently from the rest of the protein suggesting that this is the domain most likely to be S-acylated. To test this hypothesis, we inhibited S-acylation *in vivo* using 2-bromopalmitate (2-BP) (Resh, 2006). HeLaM cells were transfected with GFP-STX19$^{1-294}$ or GFP-STX19$^{275-294}$ and treated with 100 μM 2-BP overnight and the steady state distribution of the expression constructs were determined using fluorescence microscopy (**Fig. 3A and C**). In the control cells, GFP-STX19$^{1-294}$ and GFP-STX19$^{275-294}$ were localised to tubular recycling endosomes and the plasma membrane. However, in the cells treated with 100μM 2-BP the constructs became predominantly cytosolic (**Fig. 3A, C and quantified in B and D**). We also observed the levels of the constructs in the 2-BP treated samples were markedly reduced compared to the control samples and the full-length STX19 construct (GFP-STX19$^{1-294}$) was most affected. Thus, we used MG132 to inhibit the degradation of the full length

STX19 construct (GFP-STX19$^{1-294}$). This degradation phenotype is explored further in **Fig. 6**. To determine if S-acylation was also required for targeting endogenous STX19 to tubular recycling endosomes, we treated non-transfected cells with 100 µM 2-BP overnight and performed STX19 immunostaining (**Fig. 3E and quantified in F**). In control cells, STX19 is localised to tubular recycling endosomes where it co-localises with MICAL-L1. In the 2-BP treated cells STX19 staining is lost from tubular recycling endosomes. It is worth noting that this treatment also perturbs the localisation of MICAL-L1. However, a significant pool of the protein still remains associated with the tubular recycling endosomes although they appear shorter in nature. Our results suggest that S-acylation plays an important role in targeting both recombinant and endogenous STX19 to tubular recycling endosomes.

The cysteine-rich domain of STX19 is S-acylated at several sites

STX19 has eight cysteine residues with seven of them found in the conserved cysteine-rich domain at its C-terminus. To identify which of the seven cysteines are S-acylated we developed an immunoprecipitation acyl-release assay. GFP-STX19$^{1-294}$ was transfected into HEK-293T cells and then immuno-isolated using GFP-TRAP beads. The samples were reduced with TCEP (which does not affect acyl thioester bonds (Yang et al., 2010) and then alkylated to block all free (unmodified) cysteine residues. Samples were then treated with hydroxylamine at neutral pH to selectively cleave lipid-protein thioester bonds. The protein was then eluted from the resin and digested into peptides using trypsin. Digests were analysed by LC-MS/MS and S-acylated residues inferred by quantitative analysis of the relative levels of non-alkylated cysteine residues (i.e. protected from alkylation by S-acylation) with and without hydroxylamine treatment. Analysis of the mass spectrometry data for GFP-STX19$^{1-294}$ identified C-terminal tryptic peptides (VLCCWCCPCCSSK) that showed evidence of S-acylation at several sites including a peptide where Cys284, 285, 287, 288, 290 and 291 were modified (**Table S2**). However, due to technical problems we were not able to generate enough material to produce reproducible data for the different acylated forms of full length STX19. Thus, we repeated the experiments with GFP-STX19$^{275-294}$. As before we identified C-terminal tryptic peptides (VLCCWCCPCCSSK) that showed evidence of S-acylation (**Fig. 3G, H and Table S2**). Several forms of the peptide were identified including, unmodified (6 alkylated Cys), 2 S-acylation sites (4 alkylated Cys), 3 S-

acylation sites (3 alkylated Cys), 4 S-acylation sites (2 alkylated Cys), 5 S-acylation sites (1 alkylated Cys), 6 S-acylation sites (0 alkylated Cys) at a false discovery rate of 1% and a posterior error probability <0.01. Peptides containing residues predicted to be S-acylated were either exclusively identified in plus hydroxylamine treated samples or present in both plus and minus hydroxylamine treated samples but with at least a 5-fold increase in abundance after hydroxylamine treatment (**Fig. 3G**). The presence of a signal in the control (minus hydroxylamine treated samples) is likely arising from low-level loss of S-acylation during incubation steps (Jones et al., 2012). Cys284, 285, 287, 288, 290 and 291 all show evidence of S-acylation (false localisation rate of 1%) (**Fig. 3G**). However, no evidence of S-acylation was observed for Cys280. The distribution of S-acylated forms of STX19 is striking in that the majority of STX19 is S-acylated at 5 or 6 cysteines and that the fractional occupancy of S-acylation (ratio of S-acylated/total intensity of the peptide VLCCWCCPCCSSK) is high; 87% of STX19 was modified with at least 4 acyl groups (**Fig. 3G**). These results indicate that the six most C-terminal cysteine residues of STX19 can be S-acylated.

STX19 is stably associated with membranes

S-acylation is the only lipid modification that is reversible and proteomic-based approaches have measured that up to 10% of the S-acyl-proteome is actively undergoing a cycle of S-acylation and de-S-acylation (Martin et al., 2011). Thus, we wondered whether STX19 could also be cycling on and off membranes in a similar way to RAS or Ykt6 (Fukasawa et al., 2004; Lin and Conibear, 2015). To test this idea, we made use of a knock sideways approach, which is a protein re-targeting method (Robinson and Hirst, 2013). In this system, FKBP tagged peripheral proteins are re-routed on to mitochondria that are expressing an FRB domain construct in the presence of rapamycin. For example, FKBP-tagged AP2 adaptor complex is completely rerouted from the plasma membrane on to mitochondria within 10 minutes of treatment with rapamycin (Robinson et al., 2010). Thus, if STX19 is cycling on and off membranes we should be able to use this approach to re-direct it to mitochondria. HeLaM cells were transfected with FKBP-GFP (positive control), FKBP-myc-STX19[1-294] and two constructs, which cannot be S-acylated, FKBP-myc-STX19[1-277] and FKBP-myc-STX19[P1+P2+P3] (see **Fig. 5** for fuller description of this construct) . The cells were then treated with or without rapamycin for 10 minutes at 37°C and fixed and stained for the indicated

constructs. As expected, FKBP-GFP was efficiently retargeted to mitochondria (**Fig. 4A**). However, S-acylated STX19 (FKBP-myc-STX19$^{1-294}$) remained associated with the plasma membrane (**Fig. 4B**)**,** even after incubations of up to 1 hour (data not shown). We also observed that in some cells it was the mitochondria that were rerouted to the plasma membrane, suggesting that STX19 cannot be easily removed from membranes (**Fig. 4E**). When we repeated these experiments with mutant forms of STX19 that cannot be S-acylated (FKBP-myc-STX19$^{1-277}$ and FKBP-myc-STX19$^{P1+P2+P3}$) we observed that these constructs were efficiently re-targeted to mitochondria (**Fig. 4C and D**). Taken together our results indicate that S-acylated STX19 is stably associated with membranes and is not rapidly cycling on and off membranes.

Multiple acyl chains play a role in the correct targeting of STX19 to tubular recycling endosomes

The mass spectrometry experiments identified that the six most C-terminal cysteine residues of STX19 can be S-acylated. These cysteines are organised into three pairs separated by a tryptophan and a proline residue respectively (**Fig. 5A**). To gain an insight into which of the cysteines pairs are most important for STX19 targeting we have replaced them with leucine residues that cannot be S-acylated. We have generated a series of constructs where each cysteine pair (P), was mutated separately (P1, P2, and P3) or in combination (P1+2, P2+3, P1+3 and P1+2+3) (**Fig. 5A**). The cysteine pairs are numbered from the C-terminus so P1 is a construct where the most C-terminal cysteine pair has been mutated. HeLaM cells were transfected with either wild-type or mutant HA tagged STX19 constructs and then analysed by immunofluorescence microscopy (**Fig. 5B and quantified in C**). When we mutated each cysteine pair separately no significant difference was observed between the localisation of the wild-type (HA-STX19$^{1-294}$) and mutant constructs (P1, P2 and P3) consistent with there being multiple sites of S-acylation as determined by mass spectrometry. However, when we mutated several cysteine pairs simultaneously (P1+2 and P1+3) we observed a significant effect on STX19 localisation. In these mutants, STX19 is still targeted to the plasma membrane but there is a significant reduction in the number of cells showing tubular staining (**Fig. 5C**). In contrast, the construct where the last cysteine pair was intact (P2+P3) showed significant tubular staining suggesting that this cysteine pair is most

important for targeting STX19 to tubular recycling endosomes. As would be expected, the construct where all of the cysteines had been mutated (P1+2+3) behaved in a similar way to a construct where the cysteine-rich domain was deleted (HA-STX19$^{1-277}$). In both cases, the constructs were completely cytosolic and were not targeted to tubular recycling endosomes. As observed earlier, perturbing S-acylation of STX19 caused the levels of some of the mutant proteins (P1+2, P2+3, P1+3 and P1+2+3) to be reduced (**see Fig. 6A**) so longer exposure times were needed to obtain some of the images. In summary, our data suggest that the last cysteine pair (P1) is the most critical for targeting STX19 to tubular recycling endosomes. However, other cysteine pairs can compensate for its loss.

S-acylation regulates the stability of STX19

From the immunolocalisation studies, it became apparent that interfering with the S-acylation of STX19 perturbs its stability. To investigate this further, we transfected HeLaM cells with either wild-type (HA-STX19$^{1-294}$) or the mutant STX19 constructs (HA-STX19: P1, P2, P3, P1+2, P2+3, P1+3, P1+2+3, and HA-STX19$^{1-277}$) and performed immunoblotting using antibodies against HA and γ-adaptin as a loading control (**Fig. 6A and quantified in B**). As observed by microscopy, the levels of the mutant constructs, P1+2, P1+3, P1+2+3 and HA-STX19$^{1-277}$ were significantly reduced compared to wild-type STX19. We hypothesised that the mutant constructs may be degraded by ubiquitination so we repeated the experiment in the presence of the proteasomal inhibitor MG132 (Lee and Goldberg, 1998). Addition of MG132 to the cells significantly increased the levels of the mutant constructs indicating that they are being ubiquitinated and targeted for proteasomal degradation. In support of this hypothesis, we and others have identified that STX19 is ubiquitinated on several lysine residues by mass spectrometry (**Fig. S3**) (Boeing et al., 2016). Increasing the levels of the mutant constructs using MG132 does not rescue their ability to target to the plasma membrane and/or tubular recycling endosomes indicating that S-acylation is essential for this process (**Fig. S4**).

Our results suggest that when the cysteine-rich domain of STX19 is not S-acylated it becomes a novel degron. To test this hypothesis, we mutated all the cysteine pairs in a construct where the cysteine-rich domain is fused to the C-terminus of GFP (GFP-STX19^{275-}

$^{294/P1+2+3}$). HeLaM cells were transfected with GFP, GFP-STX19$^{275-294}$ or GFP-STX19$^{275-294/P1+2+3}$ and their levels determined by immunoblotting (**Fig. 6C**). The levels of GFP-STX19$^{275-294/P1+2+3}$ were significantly reduced compared to that of the wild-type STX19 reporter. As predicted, the mutant protein is not targeted to the plasma membrane or tubular recycling endosomes (**Fig. 6D**). It is possible that the degradation phenotype is simply caused by the insertion of multiple leucines within the cysteine-rich domain and does not reflect a true physiological process. To exclude this possibility, we have used the drug 2-BP to block S-acylation of the wild-type construct. HeLaM cells were transfected with GFP-STX19$^{275-294}$ and treated with increasing concentrations of 2-BP overnight. The cells were then harvested and immunoblotting performed using antibodies against GFP and γ-adaptin (**Fig. 6E and quantified in F**). The levels of the reporter construct were dramatically reduced in a dose-dependent manner suggesting that the cysteine-rich domain of STX19 is a degron that senses whether STX19 is S-acylated. Our immunoblotting results, from the truncated STX19 construct (HA-STX19$^{1-277}$), also suggest that there must be an additional degron located upstream of the cysteine-rich domain, as the truncated protein is still degraded even when the cysteine-rich domain is removed. Our results indicate that S-acylation regulates both the stability and membrane targeting of STX19.

zDHHCs 2, 3, 7, 11, and 12 are able to S-acylate STX19

S-acylation in mammals is catalysed by 23 S-acyltransferases (Fukata et al., 2004). These enzymes are polytopic membrane proteins that have a conserved zDHHC motif and are localised to various membranes including the ER, Golgi, endosomes and plasma membrane (Ohno et al., 2006). To identify which zDHHC enzymes catalyse STX19 S-acylation, we have made use of an *in vitro* assay where S-acylation is measured based on the incorporation of 17-octadecynoic acid (17-ODYA) (Martin and Cravatt, 2009; Yap et al., 2010). This label is reacted with the azide dye, IR-800 and the level of labelling quantified using an infrared imaging system. HEK-293T cells were co-transfected with GFP-STX19$^{1-294}$ and 23 different S-acyltransferases and the amount of 17-ODYA labelling quantified by measuring the ratio of IR-800 signal to GFP signal (**Fig. 7A and quantified C**). The samples were also probed for HA to verify the expression of the HA-tagged zDHHCs (**Fig. 7B**). In the control transfection (vector alone), there is a faint IR800 signal at the predicted molecular weight for GFP-

STX19$^{1-294}$, indicating that the protein is being S-acylated by the endogenous S-acyltransferases expressed in HEK-293T cells. This signal was significantly increased when zDHHCs 2, 3, 7, 11, 12 were co-transfected with STX19 suggesting that STX19 is a substrate for these enzymes (**Fig. 7C**). To determine if the cysteine-rich domain construct is also S-acylated by the same enzymes, HEK-293T cells were co-transfected GFP-STX19$^{275-294}$ and a subset of the zDHHC library (**Fig. 7D and quantified in F**). Like full length STX19, the cysteine-rich domain construct is also S-acylated by zDHHCs 2, 3, 7, 11, 12. In addition, zDHHC14 and 15 also significantly increased the IR-800 signal for this construct. These enzymes also increased the level of S-acylation of full length STX19 but the trend was not significant. To determine which of these enzymes most likely S-acylate STX19 in HeLaM cells we have examined their expression levels using microarray data (**Fig. 7H**) (Gordon et al., 2010; Kozik et al., 2013). zDHHCs 3, 7, 11 and 12 are all expressed in HeLaM cells. However, zDHHCs 2 is expressed at very low levels suggesting it is unlikely to play a major role in S-acylation in HeLaM cells. zDHHCs 3, 7, 11 and 12 are localised to the Golgi in mammalian cells (Ohno et al., 2006) suggesting that STX19 may be S-acylated at the Golgi and then traffic to the cell surface or tubular recycling endosomes. In support of this hypothesis we find that over-expression of zDHHC 3 or 7 significantly increase the Golgi localised pool of GFP-STX19$^{275-294}$ (**Fig. S5**).

Over-expressed GFP-STX19 perturbs Rab8 localisation

The precise function of STX19 is still unclear. However, endogenous STX19 shows a high degree of co-localisation with Rab8. Thus, we hypothesised that STX19 might play a role in Rab8 trafficking. To test this hypothesis, we over-expressed GFP (control), GFP-STX19$^{1-294}$ or GFP-STX19$^{1-277}$, (which cannot be S-acylated) and examined the steady-state localisation of Rab8 (**Fig. 8A and quantified in B**). In cells expressing GFP, Rab8 was localised to a range of membranous compartments, including tubular recycling endosomes, the cleavage furrow and the plasma membrane (Peranen, 2011). In cells with low to moderate levels of GFP-STX19$^{1-294}$ we found that Rab8 localisation was un-perturbed and that in many cells there was good co-localisation with GFP-STX19$^{1-294}$ (**Fig. 2D**). However, in cells with moderate to high expression levels of GFP-STX19$^{1-294}$ (1.5-fold mean intensity and above) we found Rab8 to be targeted to membrane protrusions just at or under the plasma membrane (**Fig. 8A**). In

cells over-expressing GFP-STX19$^{1-277}$, (which cannot be S-acylated), we did not observe any change in Rab8 localisation, even in cells, which had very high expression levels (5-fold mean intensity and above). Our results suggest that STX19 may have a role in Rab8 trafficking and that STX19 must be S-acylated to perturb this pathway.

DISCUSSION

STX19 is one of the least characterised Q-SNAREs in the human genome and there are only a handful of publications that have investigated its biology. Work from several labs including our own has identified that depleting STX19 using RNAi leads to defects in constitutive secretion (Gordon et al., 2010; Simpson et al., 2012) and endosome to TGN transport (Breusegem and Seaman, 2014). Biochemical studies from our group have identified that STX19 interacts with the R-SNAREs VAMPs 3 and 8 and the Q$_{bc}$ SNAREs SNAP23, 25 and 29 supporting its role in membrane fusion at the plasma membrane. In this study, we have set out to elucidate where STX19 is localised and determine how S-acylation regulates its trafficking and function.

A pool of STX19 co-localises with Rab8 and MICAL-L1

Our localisation data indicate that a pool of endogenous STX19 is localised to tubular recycling endosomes where it co-localises with Rab8 and MICAL-L1, proteins that have been shown to be involved in the endocytic recycling of proteins internalised by non-clathrin mediated endocytosis (Rahajeng et al., 2012; Sharma et al., 2009). In addition, Rab8 has also been shown to be a key player in cell polarity (Vidal-Quadras et al., 2017) and have an involvement in exocytosis (Grigoriev et al., 2011). This is the first time that a SNARE has been localised to this compartment. Currently, it is unclear whether STX19 is: a) simply recycling through this compartment back to the cell surface, b) involved in the fusion of endocytic material with the plasma membrane; or c) required for the fusion of material with tubular recycling endosomes. Over-expression of GFP-STX19 causes Rab8 positive vesicles to accumulate in membrane protrusions just at or under the plasma membrane. Our interpretation of this result is that GFP-STX19 is acting in a dominant-negative manner and

is blocking the fusion of Rab8 positive vesicles with the plasma membrane. In the future, it will be interesting to more precisely define the role of STX19 in Rab8 trafficking and cell polarity.

S-acylation regulates the levels of STX19

Inhibiting STX19 S-acylation either by genetic or chemical means causes the protein to be degraded via the proteasome. Our experimental data suggest that STX19 contains at least two degrons. The first degron is formed when the cysteine-rich domain is not S-acylated and the second is located upstream of this region. The degron present in the de-S-acylated cysteine-rich domain can efficiently target stable proteins such as GFP for degradation. At present, it is unclear what motifs or residues in STX19 are being recognised by the ubiquitination machinery. However, the cysteine-rich domain of STX19 contains several bulky hydrophobic residues (tryptophan and phenylalanine) that most likely would not normally be exposed to the cytoplasm when this region is S-acylated. Many S-acylated proteins also contain bulky hydrophobic residues in close proximity to the lipidated cysteine residues (Collins et al., 2017), suggesting that this could be a general mechanism by which de-S-acylated proteins are recognised for degradation. In the future, it will be of interest to determine if S-acylation is used as a mechanism to post-translationally regulate the levels of STX19.

STX19 is most likely S-acylated at the Golgi and then traffics to the cell surface

To identify the enzymes involved in S-acylating STX19, we performed a screen using over-expressed zDHHCs. We found that full length STX19 and the C-terminal cysteine-rich domain of STX19 are good substrates for several zDHHCs (2, 3, 7, 11 and 12) and both proteins were predominantly S-acylated by the same enzymes. This data indicates that the protein sequence of the cysteine-rich domain contains all the necessary information required for substrate recognition and S-acylation. zDHHCs 3, and 7 have been shown to have a broad substrate specificity and S-acylate proteins including HRAS, SNAP25, SNAP23, and cysteine string protein (Greaves and Chamberlain, 2011a; Greaves et al., 2010; Greaves et al., 2008;

Lu et al., 2012). However, very few substrates have been identified for zDHHC 11. Based on our expression analysis, zDHHCs 3, 7, 11 and 12 are the enzymes most likely to be involved in S-acylating STX19 in HeLaM cells. Due to the significant level of redundancy observed between these enzymes (Ohno et al., 2012), we have not attempted to further define which enzymes S-acylate STX19. All of these zDHHCs are localised to the Golgi, suggesting that STX19 is first S-acylated at the Golgi and then traffics to the plasma membrane and/or tubular recycling endosomes.

S-acylation targets STX19 and other peripheral proteins to tubular recycling endosomes

One of the most striking observations in this study is that we have identified that S-acylation is a key determinant in targeting STX19 to tubular recycling endosomes and replacing the lipid anchor with a conventional transmembrane domain, from another Q-SNARE, significantly reduces the targeting of STX19 to this compartment. This data is consistent with S-acylation acting not merely as a membrane anchor but providing information that is critical for STX19 sorting. At present, it is unclear how S-acylation targets STX19 to tubular recycling endosomes. There are several possible mechanisms: 1) S-acylation targets STX19 to lipid microdomains at the cell surface where it is subsequently internalised via non-clathrin mediated endocytosis. 2) STX19 is directly recruited to this compartment from the cytosol through a cycle of S-acylation and de-S-acylation. At present, we favour mechanism 1 because: a) there is a significant body of literature indicating that S-acylated proteins are associated with lipid microdomains at the cell surface (Chamberlain et al., 2001; Melkonian et al., 1999; Salaun et al., 2004), b) STX19 is stably associated with membranes, and c) STX19 is degraded when not S-acylated. We have observed that other S-acylated proteins (HRAS and S-acylated GFP) are also localised to tubular recycling endosomes suggesting that S-acylation may be a key factor in targeting proteins to this compartment. In the future, it will be interesting to determine how general this mechanism is and what cellular machinery is involved in sorting S-acylated proteins to this compartment.

In conclusion, we have elucidated that S-acylation is critical for targeting STX19 to tubular recycling endosomes and that this modification may have a broader role in sorting proteins to this compartment. In addition, STX19 may also prove useful for those elucidating the

mechanism of zDHHC substrate specificity, protein turnover and Rab8 dependent trafficking.

REFERENCES

Akimzhanov, A. M. and Boehning, D. (2015). Rapid and transient palmitoylation of the tyrosine kinase Lck mediates Fas signaling. *Proc Natl Acad Sci U S A* **112**, 11876-80.

Blanc, M., David, F., Abrami, L., Migliozzi, D., Armand, F., Burgi, J. and van der Goot, F. G. (2015). SwissPalm: Protein Palmitoylation database. *F1000Res* **4**, 261.

Bock, J. B., Matern, H. T., Peden, A. A. and Scheller, R. H. (2001). A genomic perspective on membrane compartment organization. *Nature* **409**, 839-41.

Boeing, S., Williamson, L., Encheva, V., Gori, I., Saunders, R. E., Instrell, R., Aygun, O., Rodriguez-Martinez, M., Weems, J. C., Kelly, G. P. et al. (2016). Multiomic Analysis of the UV-Induced DNA Damage Response. *Cell Rep* **15**, 1597-1610.

Breusegem, S. Y. and Seaman, M. N. J. (2014). Genome-wide RNAi Screen Reveals a Role for Multipass Membrane Proteins in Endosome-to-Golgi Retrieval. *Cell Rep* **9**, 1931-1945.

Chamberlain, L. H., Burgoyne, R. D. and Gould, G. W. (2001). SNARE proteins are highly enriched in lipid rafts in PC12 cells: implications for the spatial control of exocytosis. *Proc Natl Acad Sci U S A* **98**, 5619-24.

Cheeseman, L. P., Harry, E. F., McAinsh, A. D., Prior, I. A. and Royle, S. J. (2013). Specific removal of TACC3-ch-TOG-clathrin at metaphase deregulates kinetochore fiber tension. *J Cell Sci* **126**, 2102-13.

Collins, M. O., Woodley, K. T. and Choudhary, J. S. (2017). Global, site-specific analysis of neuronal protein S-acylation. *Sci Rep* **7**, 4683.

Cox, J. and Mann, M. (2008). MaxQuant enables high peptide identification rates, individualized p.p.b.-range mass accuracies and proteome-wide protein quantification. *Nat Biotechnol* **26**, 1367-72.

Crooks, G. E., Hon, G., Chandonia, J. M. and Brenner, S. E. (2004). WebLogo: a sequence logo generator. *Genome Res* **14**, 1188-90.

D'Orlando, O., Zhao, F., Kasper, B., Orinska, Z., Muller, J., Hermans-Borgmeyer, I., Griffiths, G. M., Zur Stadt, U. and Bulfone-Paus, S. (2013). Syntaxin 11 is required for NK and CD8(+) T-cell cytotoxicity and neutrophil degranulation. *Eur J Immunol* **43**, 194-208.

Duncan, J. A. and Gilman, A. G. (1998). A cytoplasmic acyl-protein thioesterase that removes palmitate from G protein alpha subunits and p21(RAS). *J Biol Chem* **273**, 15830-7.

Fukasawa, M., Varlamov, O., Eng, W. S., Sollner, T. H. and Rothman, J. E. (2004). Localization and activity of the SNARE Ykt6 determined by its regulatory domain and palmitoylation. *Proc Natl Acad Sci U S A* **101**, 4815-20.

Fukata, M., Fukata, Y., Adesnik, H., Nicoll, R. A. and Bredt, D. S. (2004). Identification of PSD-95 palmitoylating enzymes. *Neuron* **44**, 987-96.

Gordon, D. E., Bond, L. M., Sahlender, D. A. and Peden, A. A. (2010). A targeted siRNA screen to identify SNAREs required for constitutive secretion in mammalian cells. *Traffic* **11**, 1191-204.

Gordon, D. E., Chia, J., Jayawardena, K., Antrobus, R., Bard, F. and Peden, A. A. (2017). VAMP3/Syb and YKT6 are required for the fusion of constitutive secretory carriers with the plasma membrane. *PLoS Genet* **13**, e1006698.

Greaves, J. and Chamberlain, L. H. (2011a). DHHC palmitoyl transferases: substrate interactions and (patho)physiology. *Trends Biochem Sci* **36**, 245-53.

Greaves, J. and Chamberlain, L. H. (2011b). Differential palmitoylation regulates intracellular patterning of SNAP25. *J Cell Sci* **124**, 1351-60.

Greaves, J., Gorleku, O. A., Salaun, C. and Chamberlain, L. H. (2010). Palmitoylation of the SNAP25 protein family: specificity and regulation by DHHC palmitoyl transferases. *J Biol Chem* **285**, 24629-38.

Greaves, J., Salaun, C., Fukata, Y., Fukata, M. and Chamberlain, L. H. (2008). Palmitoylation and membrane interactions of the neuroprotective chaperone cysteine-string protein. *J Biol Chem* **283**, 25014-26.

Grigoriev, I., Yu, K. L., Martinez-Sanchez, E., Serra-Marques, A., Smal, I., Meijering, E., Demmers, J., Peranen, J., Pasterkamp, R. J., van der Sluijs, P. et al. (2011). Rab6, Rab8, and MICAL3 Cooperate in Controlling Docking and Fusion of Exocytotic Carriers. *Current Biology* **21**, 967-974.

Hellewell, A. L., Foresti, O., Gover, N., Porter, M. Y. and Hewitt, E. W. (2014). Analysis of familial hemophagocytic lymphohistiocytosis type 4 (FHL-4) mutant proteins reveals that S-acylation is required for the function of syntaxin 11 in natural killer cells. *PLoS One* **9**, e98900.

Jahn, R. and Scheller, R. H. (2006). SNAREs--engines for membrane fusion. *Nat Rev Mol Cell Biol* **7**, 631-43.

Jones, M. L., Collins, M. O., Goulding, D., Choudhary, J. S. and Rayner, J. C. (2012). Analysis of protein palmitoylation reveals a pervasive role in Plasmodium development and pathogenesis. *Cell Host Microbe* **12**, 246-58.

Kang, R., Wan, J., Arstikaitis, P., Takahashi, H., Huang, K., Bailey, A. O., Thompson, J. X., Roth, A. F., Drisdel, R. C., Mastro, R. et al. (2008). Neural palmitoyl-proteomics reveals dynamic synaptic palmitoylation. *Nature* **456**, 904-9.

Kloepper, T. H., Kienle, C. N. and Fasshauer, D. (2007). An elaborate classification of SNARE proteins sheds light on the conservation of the eukaryotic endomembrane system. *Mol Biol Cell* **18**, 3463-71.

Kozik, P., Hodson, N. A., Sahlender, D. A., Simecek, N., Soromani, C., Wu, J., Collinson, L. M. and Robinson, M. S. (2013). A human genome-wide screen for regulators of clathrin-coated vesicle formation reveals an unexpected role for the V-ATPase. *Nat Cell Biol* **15**, 50-60.

Lee, D. H. and Goldberg, A. L. (1998). Proteasome inhibitors: valuable new tools for cell biologists. *Trends Cell Biol* **8**, 397-403.

Lin, D. T. and Conibear, E. (2015). ABHD17 proteins are novel protein depalmitoylases that regulate N-Ras palmitate turnover and subcellular localization. *Elife* **4**, e11306.

Linder, M. E. and Deschenes, R. J. (2007). Palmitoylation: policing protein stability and traffic. *Nat Rev Mol Cell Biol* **8**, 74-84.

Lu, D., Sun, H. Q., Wang, H., Barylko, B., Fukata, Y., Fukata, M., Albanesi, J. P. and Yin, H. L. (2012). Phosphatidylinositol 4-kinase IIalpha is palmitoylated by Golgi-localized palmitoyltransferases in cholesterol-dependent manner. *J Biol Chem* **287**, 21856-65.

Martin, B. R. and Cravatt, B. F. (2009). Large-scale profiling of protein palmitoylation in mammalian cells. *Nat Methods* **6**, 135-8.

Martin, B. R., Wang, C., Adibekian, A., Tully, S. E. and Cravatt, B. F. (2011). Global profiling of dynamic protein palmitoylation. *Nat Methods* **9**, 84-9.

Matsuda, T. and Cepko, C. L. (2007). Controlled expression of transgenes introduced by in vivo electroporation. *Proc Natl Acad Sci U S A* **104**, 1027-32.

Melkonian, K. A., Ostermeyer, A. G., Chen, J. Z., Roth, M. G. and Brown, D. A. (1999). Role of lipid modifications in targeting proteins to detergent-resistant membrane rafts. Many raft proteins are acylated, while few are prenylated. *J Biol Chem* **274**, 3910-7.

Misaki, R., Morimatsu, M., Uemura, T., Waguri, S., Miyoshi, E., Taniguchi, N., Matsuda, M. and Taguchi, T. (2010). Palmitoylated Ras proteins traffic through recycling endosomes to the plasma membrane during exocytosis. *J Cell Biol* **191**, 23-9.

Muszbek, L., Haramura, G., Cluette-Brown, J. E., Van Cott, E. M. and Laposata, M. (1999). The pool of fatty acids covalently bound to platelet proteins by thioester linkages can be altered by exogenously supplied fatty acids. *Lipids* **34 Suppl**, S331-7.

Ohno, Y., Kashio, A., Ogata, R., Ishitomi, A., Yamazaki, Y. and Kihara, A. (2012). Analysis of substrate specificity of human DHHC protein acyltransferases using a yeast expression system. *Mol Biol Cell* **23**, 4543-51.

Ohno, Y., Kihara, A., Sano, T. and Igarashi, Y. (2006). Intracellular localization and tissue-specific distribution of human and yeast DHHC cysteine-rich domain-containing proteins. *Biochim Biophys Acta* **1761**, 474-83.

Page, L. J. and Robinson, M. S. (1995). Targeting signals and subunit interactions in coated vesicle adaptor complexes. *J Cell Biol* **131**, 619-30.

Peranen, J. (2011). Rab8 GTPase as a regulator of cell shape. *Cytoskeleton (Hoboken)* **68**, 527-39.

Prekeris, R., Klumperman, J. and Scheller, R. H. (2000). Syntaxin 11 is an atypical SNARE abundant in the immune system. *Eur J Cell Biol* **79**, 771-80.

Rahajeng, J., Giridharan, S. S., Cai, B., Naslavsky, N. and Caplan, S. (2012). MICAL-L1 is a tubular endosomal membrane hub that connects Rab35 and Arf6 with Rab8a. *Traffic* **13**, 82-93.

Resh, M. D. (2006). Use of analogs and inhibitors to study the functional significance of protein palmitoylation. *Methods* **40**, 191-7.

Robinson, M. S. and Hirst, J. (2013). Rapid inactivation of proteins by knocksideways. *Curr Protoc Cell Biol* **61**, 15 20 1-7.

Robinson, M. S., Sahlender, D. A. and Foster, S. D. (2010). Rapid inactivation of proteins by rapamycin-induced rerouting to mitochondria. *Dev Cell* **18**, 324-31.

Rothbauer, U., Zolghadr, K., Muyldermans, S., Schepers, A., Cardoso, M. C. and Leonhardt, H. (2008). A versatile nanotrap for biochemical and functional studies with fluorescent fusion proteins. *Mol Cell Proteomics* **7**, 282-9.

Salaun, C., James, D. J. and Chamberlain, L. H. (2004). Lipid rafts and the regulation of exocytosis. *Traffic* **5**, 255-64.

Schmick, M., Vartak, N., Papke, B., Kovacevic, M., Truxius, D. C., Rossmannek, L. and Bastiaens, P. I. H. (2014). KRas localizes to the plasma membrane by spatial cycles of solubilization, trapping and vesicular transport. *Cell* **157**, 459-471.

Schneider, T. D. and Stephens, R. M. (1990). Sequence logos: a new way to display consensus sequences. *Nucleic Acids Res* **18**, 6097-100.

Sharma, M., Giridharan, S. S., Rahajeng, J., Naslavsky, N. and Caplan, S. (2009). MICAL-L1 links EHD1 to tubular recycling endosomes and regulates receptor recycling. *Mol Biol Cell* **20**, 5181-94.

Simpson, J. C., Joggerst, B., Laketa, V., Verissimo, F., Cetin, C., Erfle, H., Bexiga, M. G., Singan, V. R., Heriche, J. K., Neumann, B. et al. (2012). Genome-wide RNAi screening identifies human proteins with a regulatory function in the early secretory pathway. *Nat Cell Biol* **14**, 764-74.

Smotrys, J. E. and Linder, M. E. (2004). Palmitoylation of intracellular signaling proteins: regulation and function. *Annu Rev Biochem* **73**, 559-87.

Tomatis, V. M., Trenchi, A., Gomez, G. A. and Daniotti, J. L. (2010). Acyl-protein thioesterase 2 catalyzes the deacylation of peripheral membrane-associated GAP-43. *PLoS One* **5**, e15045.

Vidal-Quadras, M., Holst, M. R., Francis, M. K., Larsson, E., Hachimi, M., Yau, W. L., Peranen, J., Martin-Belmonte, F. and Lundmark, R. (2017). Endocytic turnover of Rab8 controls cell polarization. *J Cell Sci* **130**, 1147-1157.

Wang, Y., Foo, L. Y., Guo, K., Gan, B. Q., Zeng, Q., Hong, W. and Tang, B. L. (2006). Syntaxin 9 is enriched in skin hair follicle epithelium and interacts with the epidermal growth factor receptor. *Traffic* **7**, 216-26.

Wen, W., Yu, J., Pan, L., Wei, Z., Weng, J., Wang, W., Ong, Y. S., Tran, T. H., Hong, W. and Zhang, M. (2010). Lipid-Induced conformational switch controls fusion activity of longin domain SNARE Ykt6. *Mol Cell* **37**, 383-95.

Yang, W., Di Vizio, D., Kirchner, M., Steen, H. and Freeman, M. R. (2010). Proteome scale characterization of human S-acylated proteins in lipid raft-enriched and non-raft membranes. *Mol Cell Proteomics* **9**, 54-70.

Yap, M. C., Kostiuk, M. A., Martin, D. D., Perinpanayagam, M. A., Hak, P. G., Siddam, A., Majjigapu, J. R., Rajaiah, G., Keller, B. O., Prescher, J. A. et al. (2010). Rapid and selective detection of fatty acylated proteins using omega-alkynyl-fatty acids and click chemistry. *J Lipid Res* **51**, 1566-80.

Yokoi, N., Fukata, Y., Sekiya, A., Murakami, T., Kobayashi, K. and Fukata, M. (2016). Identification of PSD-95 Depalmitoylating Enzymes. *J Neurosci* **36**, 6431-44.

zur Stadt, U., Schmidt, S., Kasper, B., Beutel, K., Diler, A. S., Henter, J. I., Kabisch, H., Schneppenheim, R., Nurnberg, P., Janka, G. et al. (2005). Linkage of familial hemophagocytic lymphohistiocytosis (FHL) type-4 to chromosome 6q24 and identification of mutations in syntaxin 11. *Hum Mol Genet* **14**, 827-34.

Figures
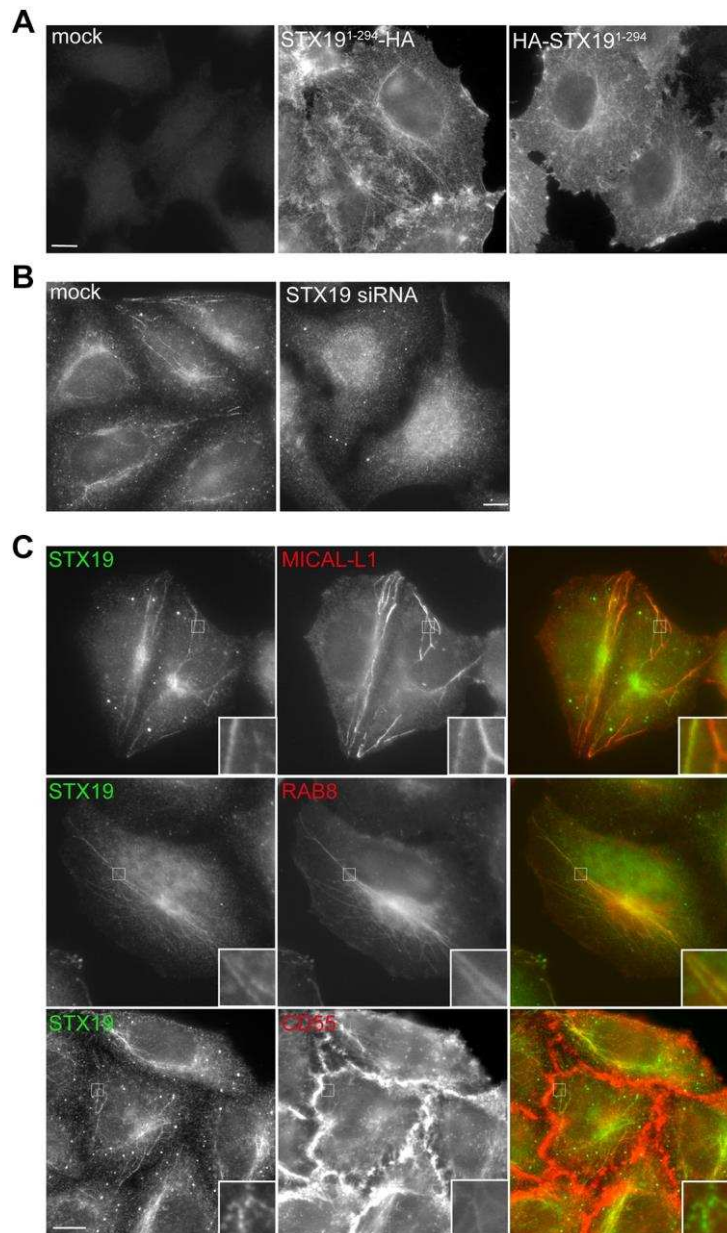
Figure 1. A pool of STX19 is localised to the plasma membrane and branched tubular membranes. A) HeLaM cells were seeded onto coverslips, transfected with either HA-STX19 or STX19-HA and grown overnight. The cells were then fixed and stained with antibodies against HA. **B)** HeLaM cells were either mock transfected or transfected with siRNA targeting STX19 using a 96 hour double transfection protocol. The cells were seeded onto coverslips, fixed and stained with antibodies against STX19. **C)** HeLaM cells were seeded onto coverslips

and grown overnight. The cells were fixed and stained with antibodies against STX19 and MICAL-L1. HeLaM cells were seeded onto coverslips, transfected with Strawberry-Rab8 and grown overnight. The cells were then fixed and stained with antibodies against STX19. HeLaM cells were seeded onto coverslips and grown overnight. The next day the cells were incubated with antibodies against CD55 for 1 hour at 37°C. The cells were then fixed and stained with antibodies against STX19. Scale bar 10 µm.
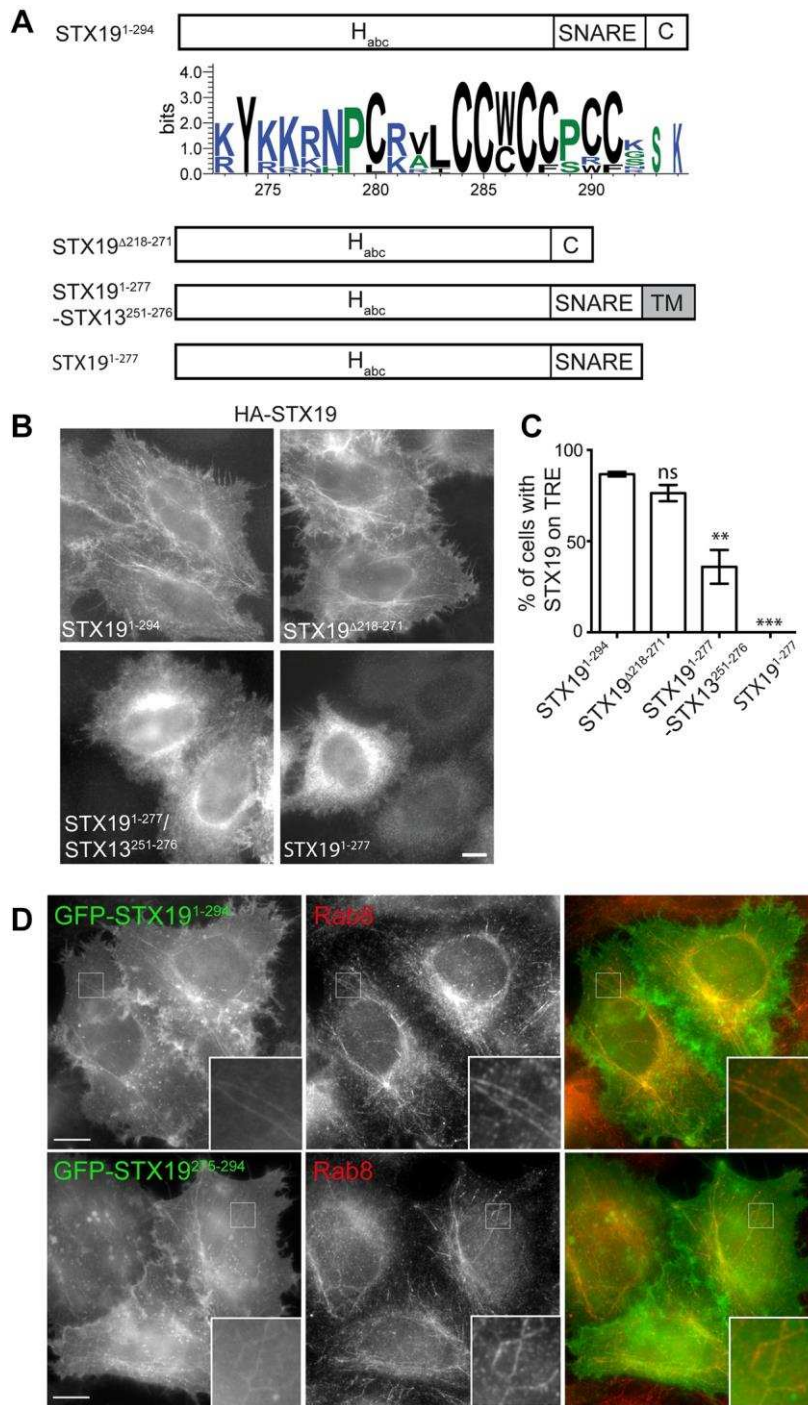
Figure 2. The C-terminal cysteine-rich domain of STX19 is essential for targeting STX19 to tubular recycling endosomes. A) Diagrammatic representation of STX19 and the expression constructs used in this figure. The position of the predicted H_{abc} domain, SNARE motif, cysteine-rich domain (C) and transmembrane domain (TM) have been highlighted. A sequence alignment was performed using the cysteine-rich domain and a graphical representation of the sequence conservation generated by WebLogo 3 (Crooks et al., 2004;

Schneider and Stephens, 1990). The x-axis shows the position of each amino acid in the cysteine-rich domain and the height of the y-axis indicates the information content at each position (measured in bits). Amino acids are colour coded as follows; blue for charged, black for hydrophobic and green for polar. **B)** To determine which domains of STX19 are important for targeting STX19 to membranes, HeLaM cells were transfected with the indicated HA tagged expression constructs. The cells were then fixed and stained with antibodies against HA and Rab8 (the representative Rab8 images can be seen in **Fig. S1**). **C)** The efficiency by which the STX19 constructs were targeted to this compartment were manually quantified by counting the number of cells that showed STX19 staining that co-localised with Rab8. Between 50 and 100 cells were imaged for each construct. Error bars show the SEM for three independent experiments. The P values for each sample were calculated (** indicates P ≤ 0.01 and *** ≤ 0.001). **D)** HeLaM cells were transfected with GFP-STX19$^{1-294}$ or GFP-STX19$^{275-294}$, fixed and stained with antibodies against Rab8. Scale bar 10 μm.
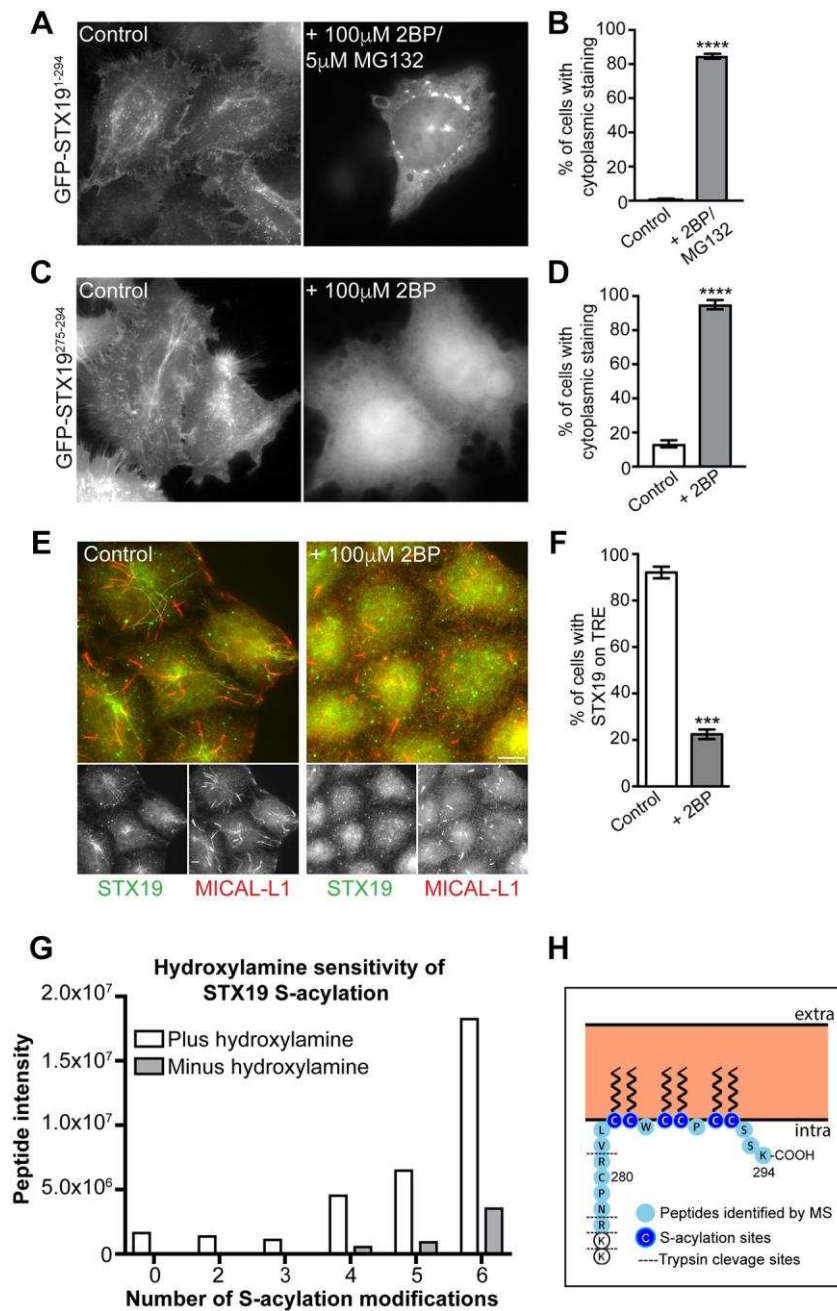
Figure 3. The cysteine-rich domain of STX19 is S-acylated on multiple cysteines and this modification is critical for targeting STX19 to the plasma membrane and tubular recycling endosomes.

A-D) To determine if recombinant STX19 was S-acylated *in vivo,* HelaM cells were transfected with either GFP-STX19$^{1-294}$ or GFP-STX19$^{275-294}$ and treated with 100 µM 2-BP for 16 hours. The cells were then fixed and imaged. Scale bar 10 µm. To quantify the effect of 2-

BP treatment on the STX19 expression constructs, between 50 and 100 cells were counted and the number of cells with cytoplasmic STX19 staining quantified. Error bars show the SEM from three independent experiments. The P values for each sample were calculated (**** indicates P ≤ 0.0001). **E and F)** To determine if endogenous STX19 is S-acylated *in vivo,* HeLaM cells were grown on coverslips overnight and treated with 100 µM 2-BP for 16 hours. The cells were then fixed and stained with antibodies against STX19 and MICAL-L1. To quantify the effect of 2-BP on STX19 localisation, between 50 and 100 cells were counted and the number of cells with tubular STX19 staining quantified (as defined by overlap with MICAL-L1 positive tubules). Error bars show the SEM from three independent experiments. The P values for each sample were calculated (*** indicates P ≤ ≤ 0.001). **G)** To identify which cysteine residues of STX19 are S-acylated, immuno-isolated GFP-STX19[275-294] was reduced, alkylated and treated (+/- 1 M hydroxylamine) to cleave thioester bonds. The samples were then digested with trypsin and the resulting peptides quantified using mass spectrometry. The hydroxylamine sensitivity of the cysteine residues was determined by measuring the relative intensity (extracted ion chromatogram) non-alkylated peptides in the presence or absence of hydroxylamine. **H)** Diagram showing the position and sequence of the tryptic peptide identified by mass spectrometry that shows evidence of S-acylation. The positions of the individual S-acylation sites are marked in dark blue.
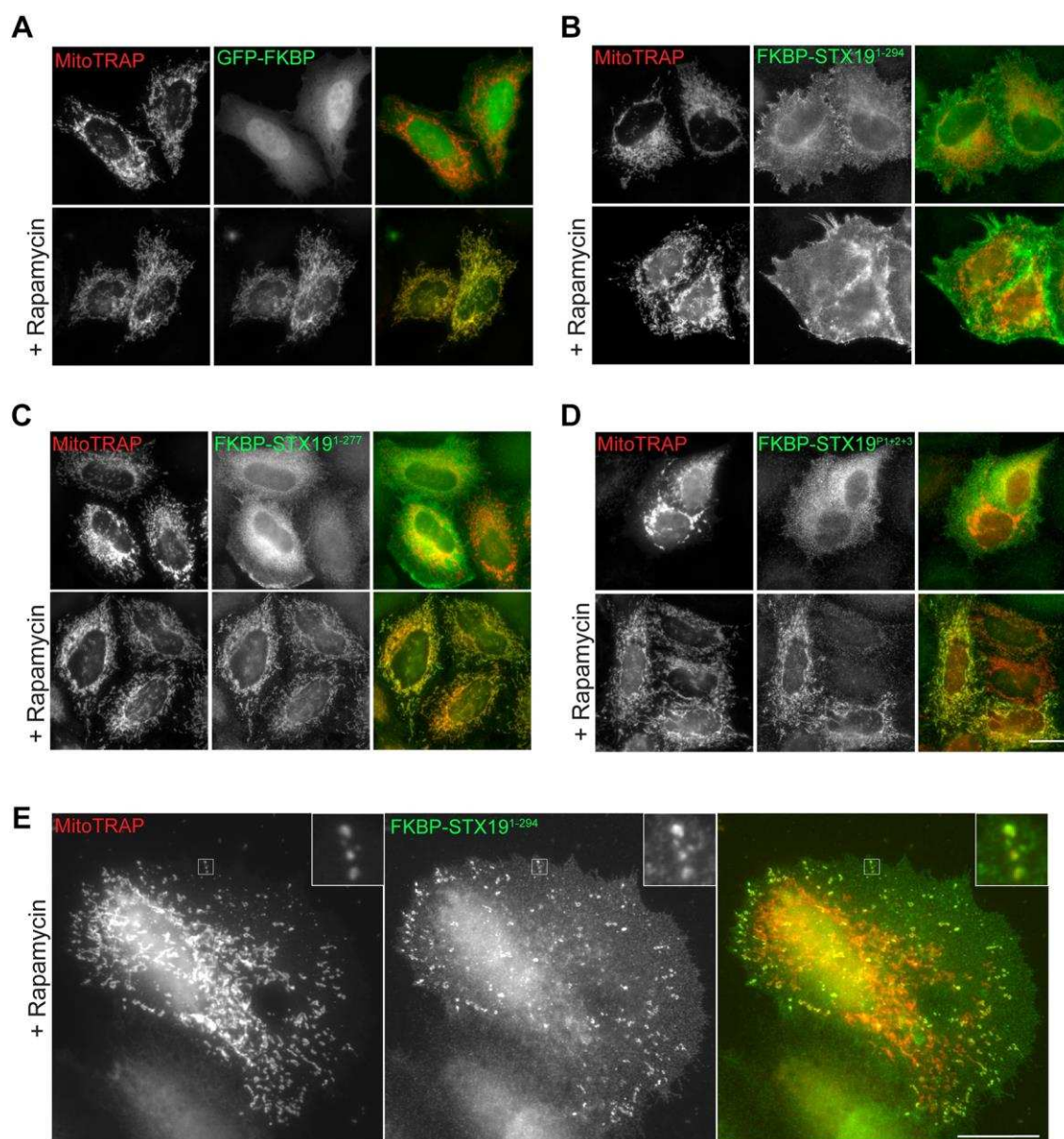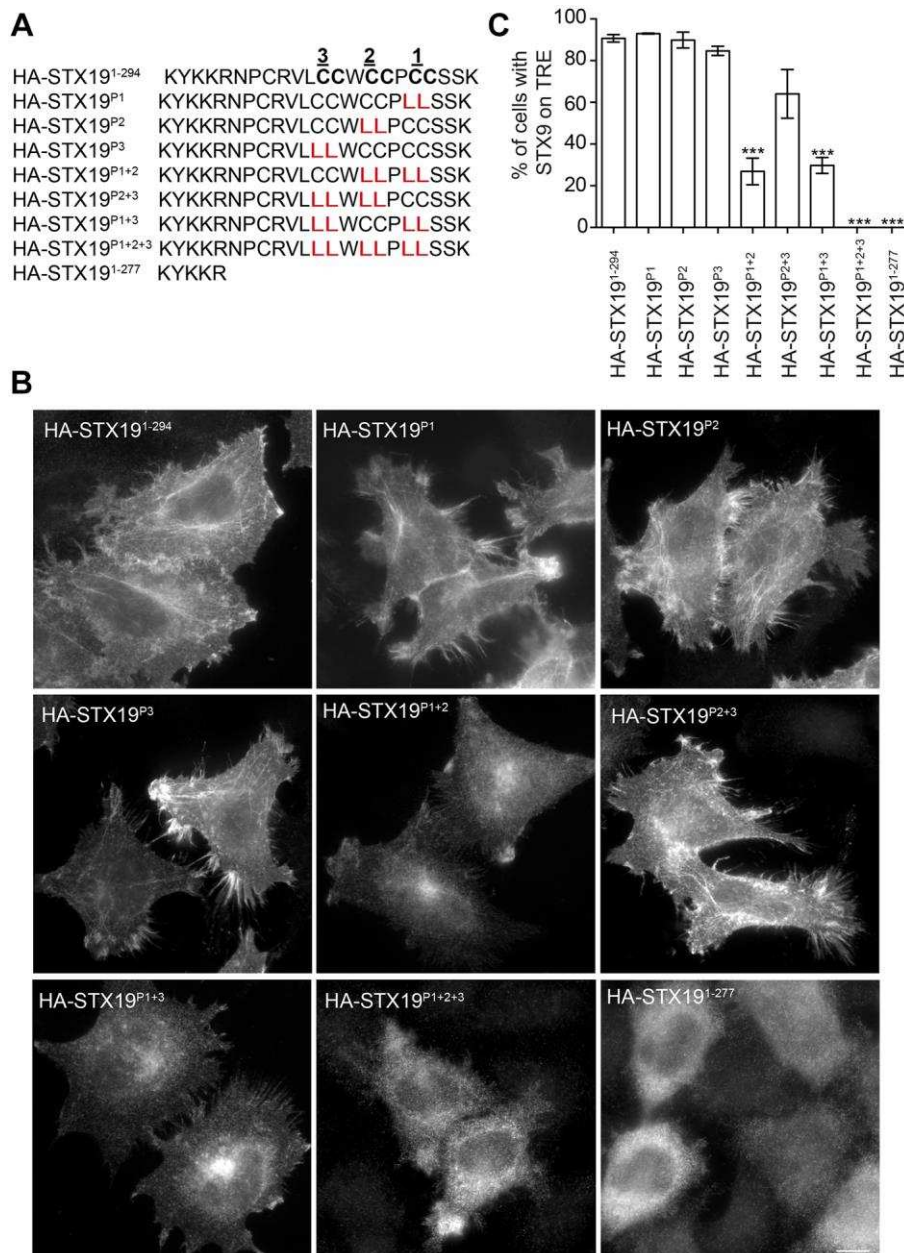
**Figure 4. STX19 is stably associated with membranes**

To determine if STX19 is cycling on and off membranes we have made use of the knock sideways approach. HeLaM cells were co-transfected with MitoTRAP (Mito-mCherry-FRB) and either FKBP-GFP (positive control)(**A**), FKBP-myc-STX19$^{1\text{-}294}$ (**B**), FKBP-myc-STX19$^{1\text{-}277}$ (**C**) and FKBP-myc-STX19$^{P1+P2+P3}$ (construct in which all the cysteines have been mutated to leucine)(**D**). 24 hours post-transfection the cells were then treated with or without 1 µM rapamycin for 10 minutes. The cells were then fixed and stained with antibodies against myc. Scale bar 10 µm. **E**) HeLaM cells were co-transfected with MitoTRAP (Mito-mCherry-

FRB) and FKBP-myc-STX19$^{1-294}$. 24 hours post transfection the cells were then treated with or without 1 μM rapamycin for 10 minutes. The cells were then fixed and stained with antibodies against myc. Scale bar 20 μm.

A

```
                                            3   2   1
HA-STX19¹⁻²⁹⁴   KYKKRNPCRVLCCWCCPCCSSK
HA-STX19ᴾ¹      KYKKRNPCRVLCCWCCPLLSSK
HA-STX19ᴾ²      KYKKRNPCRVLCCWLLPCCSSK
HA-STX19ᴾ³      KYKKRNPCRVLLLWCCPCCSSK
HA-STX19ᴾ¹⁺²    KYKKRNPCRVLCCWLLPLLSSK
HA-STX19ᴾ²⁺³    KYKKRNPCRVLLLWLLPCCSSK
HA-STX19ᴾ¹⁺³    KYKKRNPCRVLLLWCCPLLSSK
HA-STX19ᴾ¹⁺²⁺³  KYKKRNPCRVLLLWLLPLLSSK
HA-STX19¹⁻²⁷⁷   KYKKR
```

C

B

Figure 5. Multiple cysteines are required for the correct targeting of STX19 to the plasma membrane and tubular recycling endosomes. A) The C-terminal sequence of the STX19 expression constructs used in this figure are shown. The positions of the mutant residues are highlighted in red. The cysteine pairs were numbered from the C-terminus. **B)** HeLaM cells were grown overnight on coverslips and then transfected with the indicated STX19 constructs. 24 hours post-transfection, the cells were fixed and stained for HA and Rab8. For

simplicity, only the HA staining is shown. Scale bar 10 μm. **C)** To quantify the effect of these mutations on STX19 membrane targeting, between 50 and 100 cells were counted for each construct and the percentage of cells showing STX19 staining on tubular recycling endosomes quantified (as defined by overlap with Rab8 positive tubules). Error bar shows SEM from three independent repeats. The P values for each sample were calculated (*** indicates P ≤ 0.001).
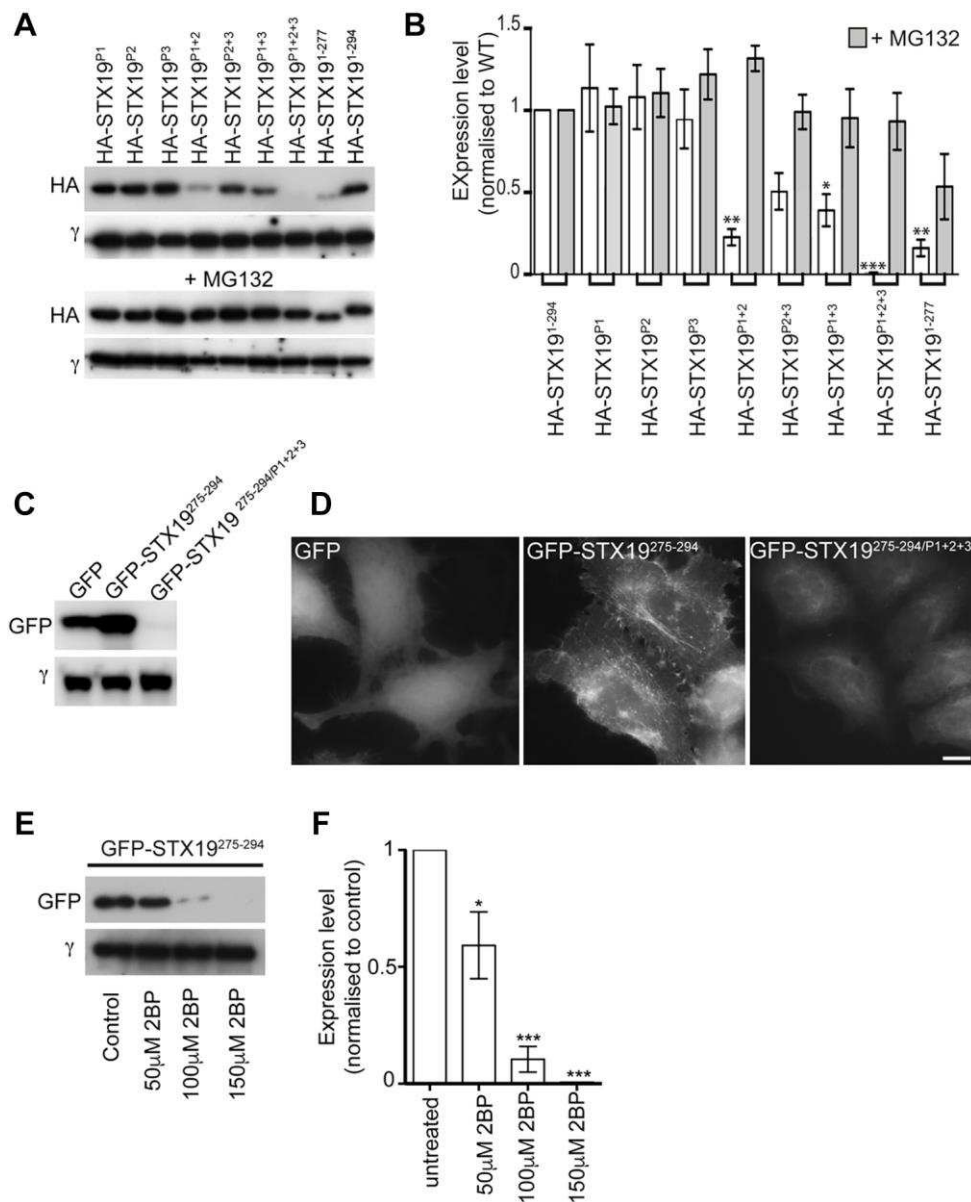
Figure 6. S-acylation regulates the stability of STX19. A) HeLaM cells were grown overnight and transfected with the indicated HA-STX19 constructs. 8 hours post-transfection, the cells were treated with or without 5 µM MG132. 16 hours later the cells were harvested, cell lysates prepared, separated by SDS-PAGE and transferred onto membranes. The membranes were then probed for HA and γ-adaptin as a loading control. **B)** Western blots from three independent experiments were quantified. Error bars show the SEM from three independent repeats. The P values for each sample were calculated (** indicates P ≤ 0.01 and *** ≤ 0.001). **C)** HeLaM cells were transfected with either GFP, GFP-STX19$^{275-294}$ or GFP-

STX19$^{275-294/P1+2+3}$. 24 hours post-transfection cell extracts were prepared from the cells, separated by SDS-PAGE and transferred onto PVDF membranes. The membranes were then probed for GFP and γ-adaptin as a loading control. **D)** HeLaM cells were grown on coverslips and transfected with GFP, GFP-STX19$^{275-294}$ or GFP-STX19$^{275-294/P1+2+3}$. 24 hours post-transfection the cells were fixed and imaged. Scale bar 10 μm. **E)** HeLaM cells were transfected with GFP-STX19$^{275-294}$. 8 hours post-transfection the cells were treated with the indicated concentrations of 2-BP. 16 hours later, cell extracts were prepared from the cells, separated by SDS-PAGE and transferred onto PVDF membranes. The membranes were then probed for GFP and γ-adaptin as a loading control. **F)** Western blots from three independent experiments were quantified. Error bars show the SEM from three independent experiments. The P values for each sample were calculated (* indicates P ≤ 0.05; and ******* ≤ 0.001).
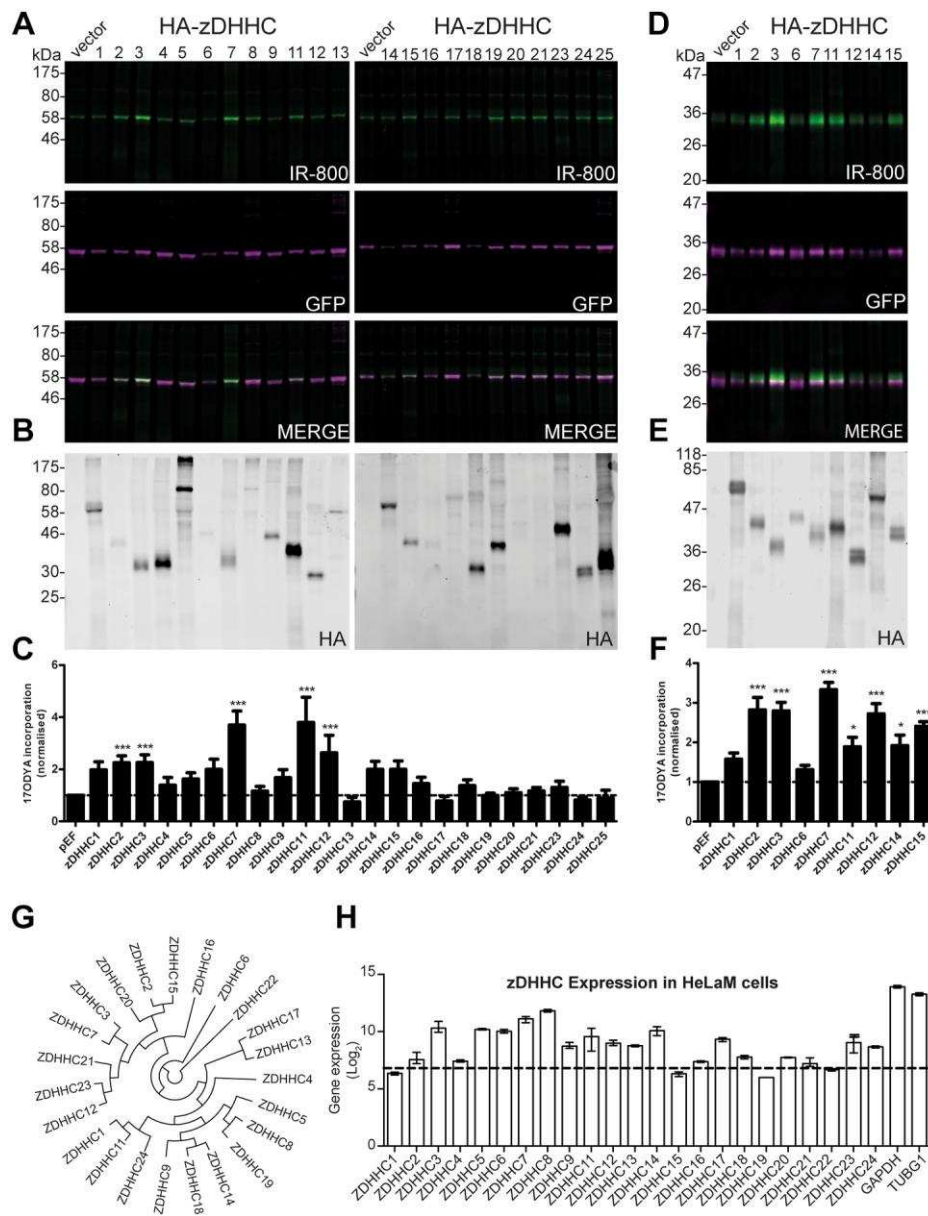
Figure 7. zDHHCs 2, 3, 7, 11 and 12 are capable of S-acylating STX19. HEK-293T cells were grown overnight and co-transfected with 23 HA-tagged S-acyltransferases and either GFP-STX19$^{1-294}$ (**A-C**) or GFP-STX19$^{275-294}$ (**D-F**). 24 hours post-transfection, the cells were labelled with 100 μM 17-octadecynoic acid (17-ODYA) for 3 hours at 37°C. The cells were washed, lysed and incubated with the click reaction buffer containing azide IR800 dye for 1 hour. The samples were then acetone precipitated and resuspended in 1X Laemmli sample buffer. The samples were then separated by SDS-PAGE and transferred onto nitrocellulose membranes for blotting with antibodies against HA or GFP. **A and D**) Representative images showing the

expression levels of the GFP-STX19 constructs and the level of IR-800 labelling for each transfection. The third panel shows the merged image for both channels. **B and E**) Representative images showing the expression levels of the HA tagged S-acyltransferases for each transfection. **C and F**) The level of 17-ODYA incorporation was calculated and normalised to the vector control. Error bars show SEM and the data from six independent experiments were used. The P values for each sample were calculated (* indicates P < 0.05 and ******* < 0.001). **G)** Diagram representing the phylogenetic relationship of the mammalian S-acyltransferases. **H)** To estimate the expression levels of the S-acyltransferases in HeLaM cells, previously published microarray data was re-analysed (Gordon et al., 2010; Kozik et al., 2013). The dotted line indicates the minimum level of signal that represents significant gene expression. Error bars show the experimental range for six independent biological repeats.
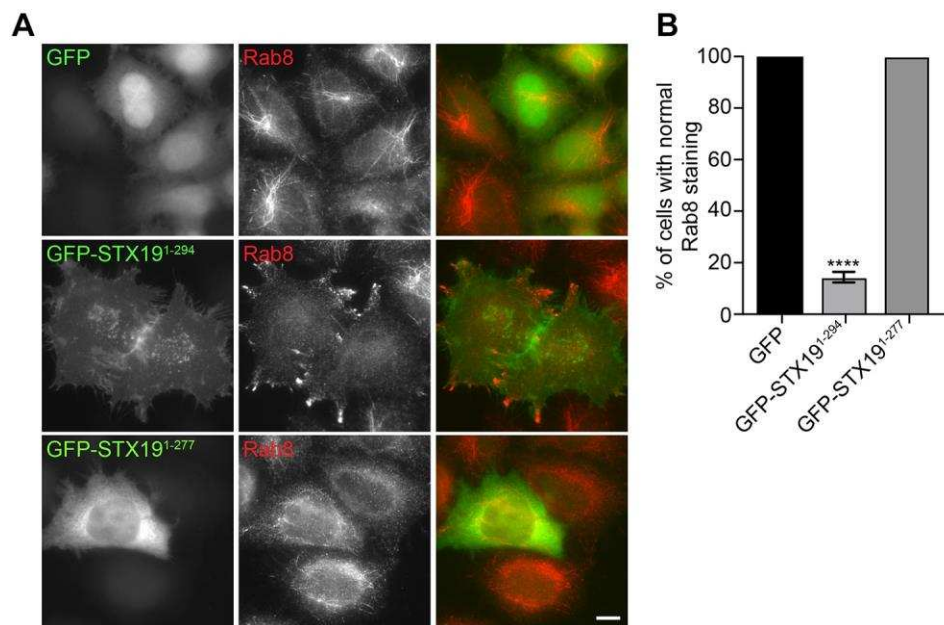
Figure 8. Over-expression of S-acylated GFP-STX19 perturbs the localisation of Rab8.

HeLaM cells were grown overnight and transfected with either GFP, GFP-STX19$^{1-294}$ or GFP-STX19$^{1-277}$ (which lacks the cysteine rich domain). 24 hours post-transfection, the cells were fixed and stained for Rab8 (**A**). Scale bar 10 µm. To quantify the effect of the various constructs on Rab8 localisation, between 50 and 100 cells were counted. Error bars show the SEM from three independent experiments (**B**). The P values for each sample were calculated (**** indicates P ≤ 0.0001).
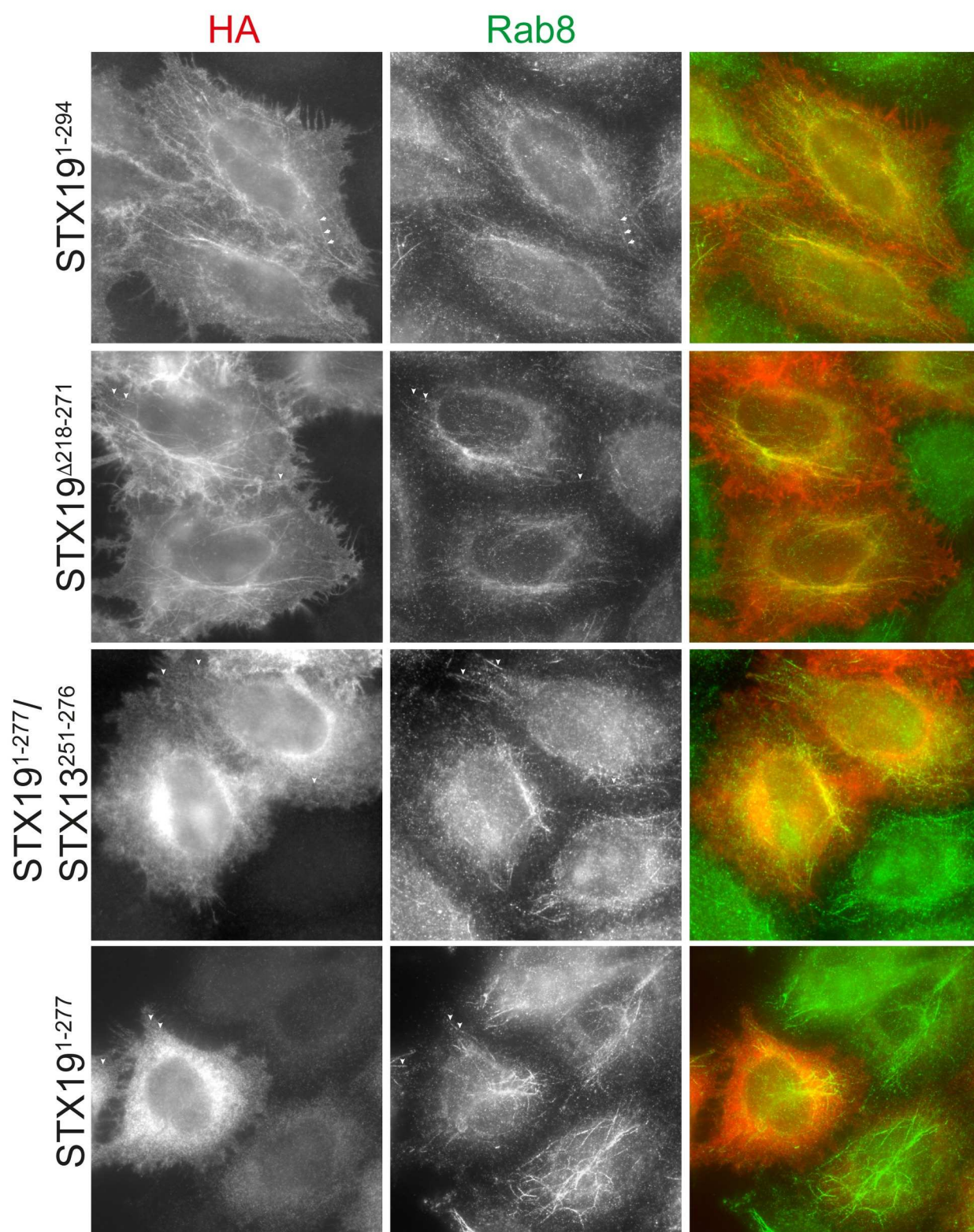
Fig. S1. The C-terminal cysteine-rich domain of STX19 is required for targeting STX19 to tubular recycling endosomes. HeLaM cells were grown on coverslips overnight and transfected with the indicated HA-STX19 expression constructs. The cells were then fixed and stained with antibodies against HA and Rab8. Arrowheads indicate the position of Rab8 tubules. Scale bar 10 μm.
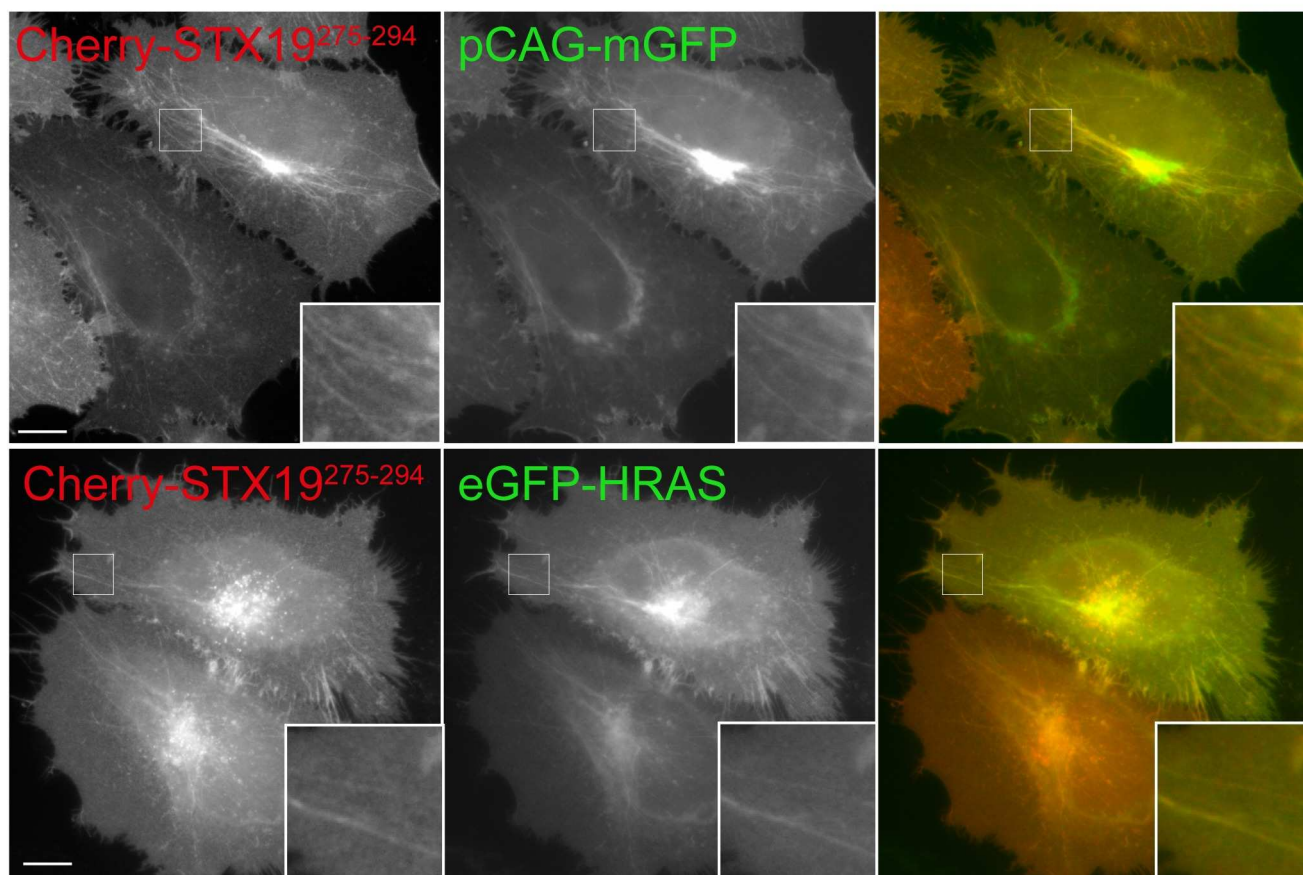
Fig. S2. Other S-acylated proteins are efficiently targeted to tubular recycling endosomes. HeLaM cells were co-transfected with mCherry-STX19[275-294] and GFP-HRAS or pCAG-mGFP (GFP fused with GAP43 S-acylation sequence). The cells were fixed 24 hours post transfection and mounted onto slides. Scale bar 10 μm.

a)

b)
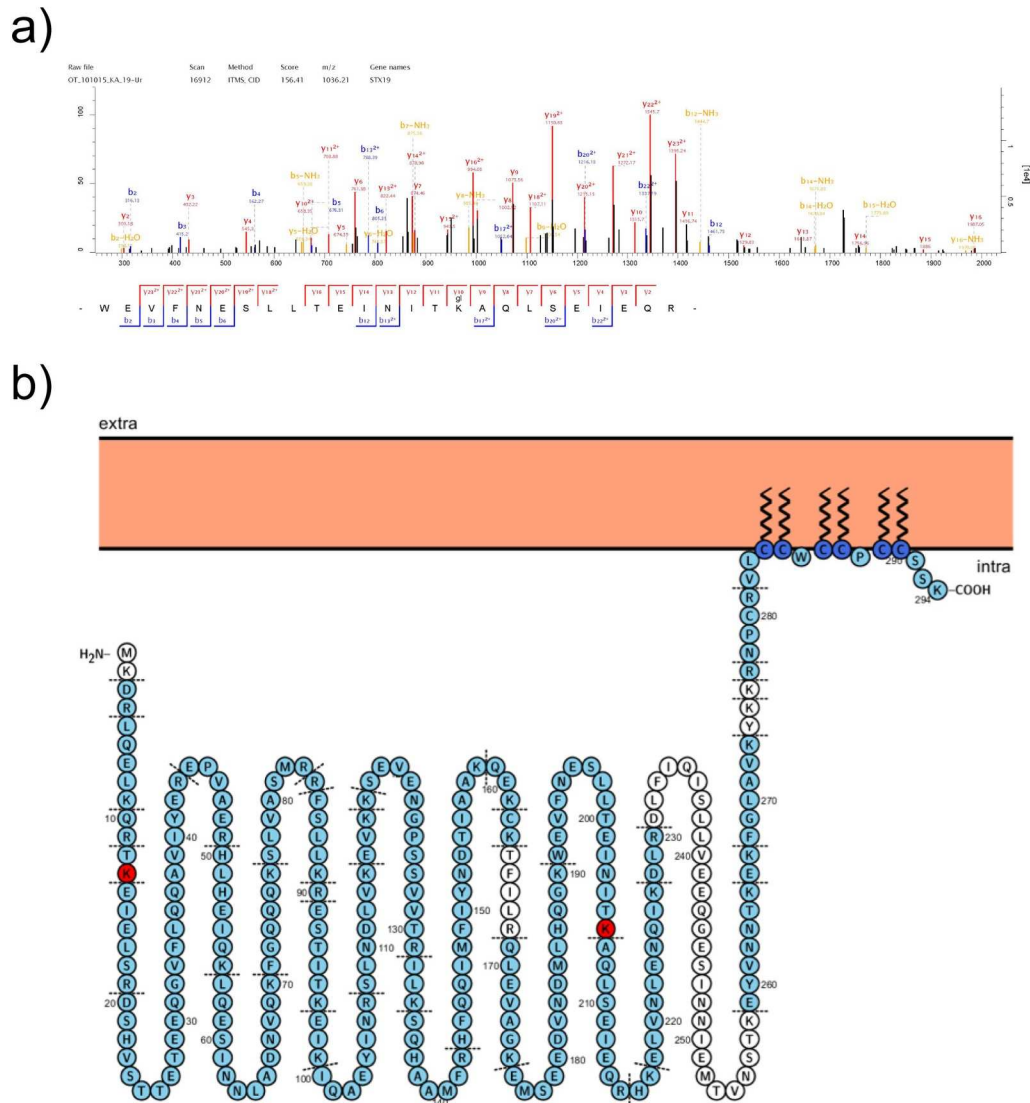
Fig. S3. STX19 is ubiquitinated at several lysine residues. To identify which residues of STX19 are ubiquitinated, HeLaM cells were transfected with GFP-STX19[1-294] and incubated with 5 μM MG132 for 8 hours. The cells were lysed and STX19 immunoisolated using GFP-TRAP beads. STX19 was then digested using trypsin and the resulting peptides analysed using LC-MS/MS. A) Representative fragmentation spectrum showing identification of K206 as a site of ubiquitination. B) Diagram showing the position of ubiquitinated lysine residues in STX19 marked in red (K13 PhosphoSitePlus data and K206 our experimental data). Residues shaded in light blue indicate which peptides were detected by MS analysis of GFP-STX9 IPs.
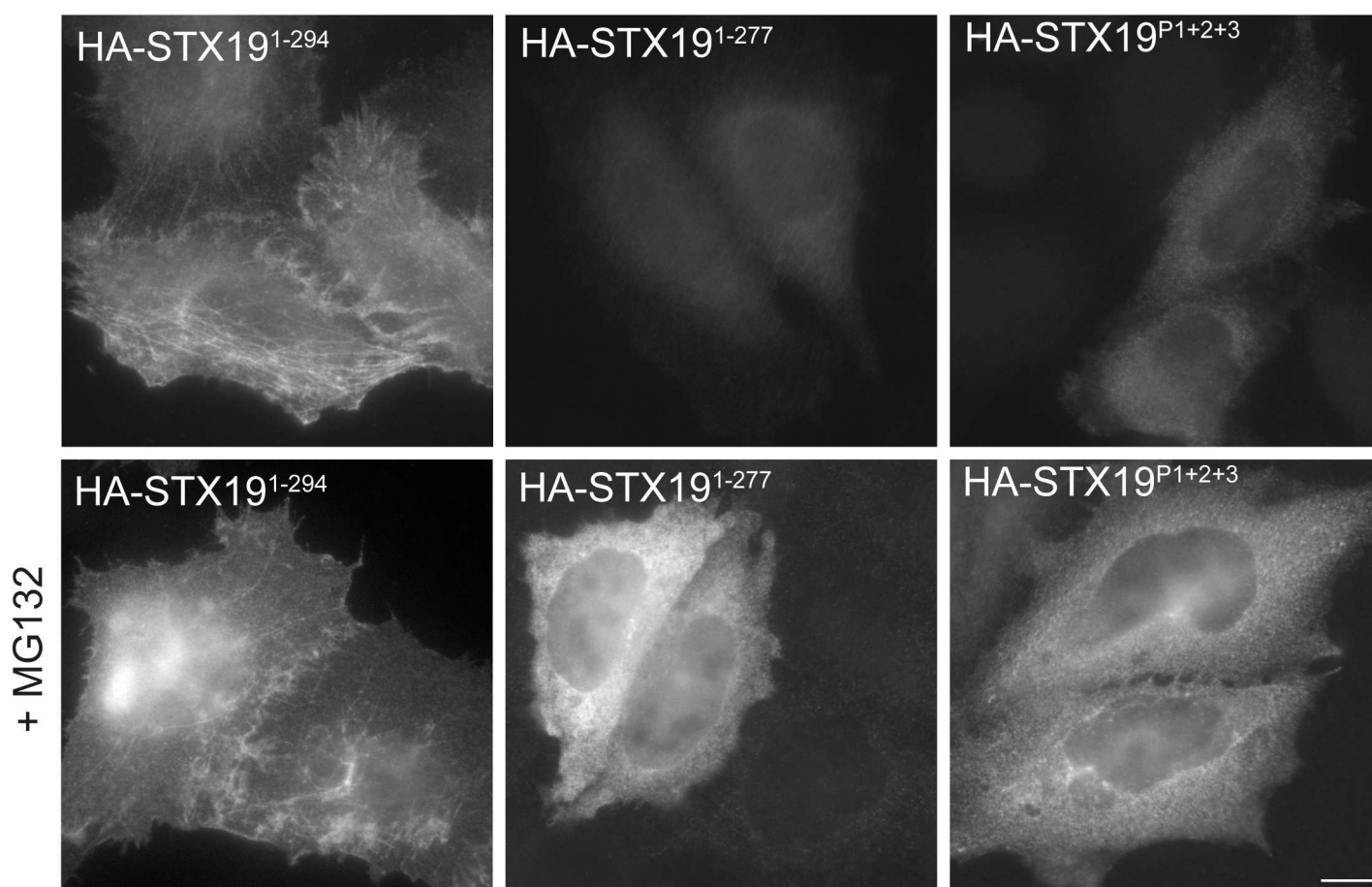
Fig. S4. Proteasomal inhibition does not rescue the membrane association of mutant STX19 constructs. HeLaM cells were grown overnight and transfected with the indicated HA-STX19 constructs. 8 hours post-transfection, the cells were treated with or without 5 μM MG132 for a further 8 hours. The cells were then fixed and stained with antibodies against HA. Scale bar 10 μm. The same exposure times were used for the cells treated with or without MG132.
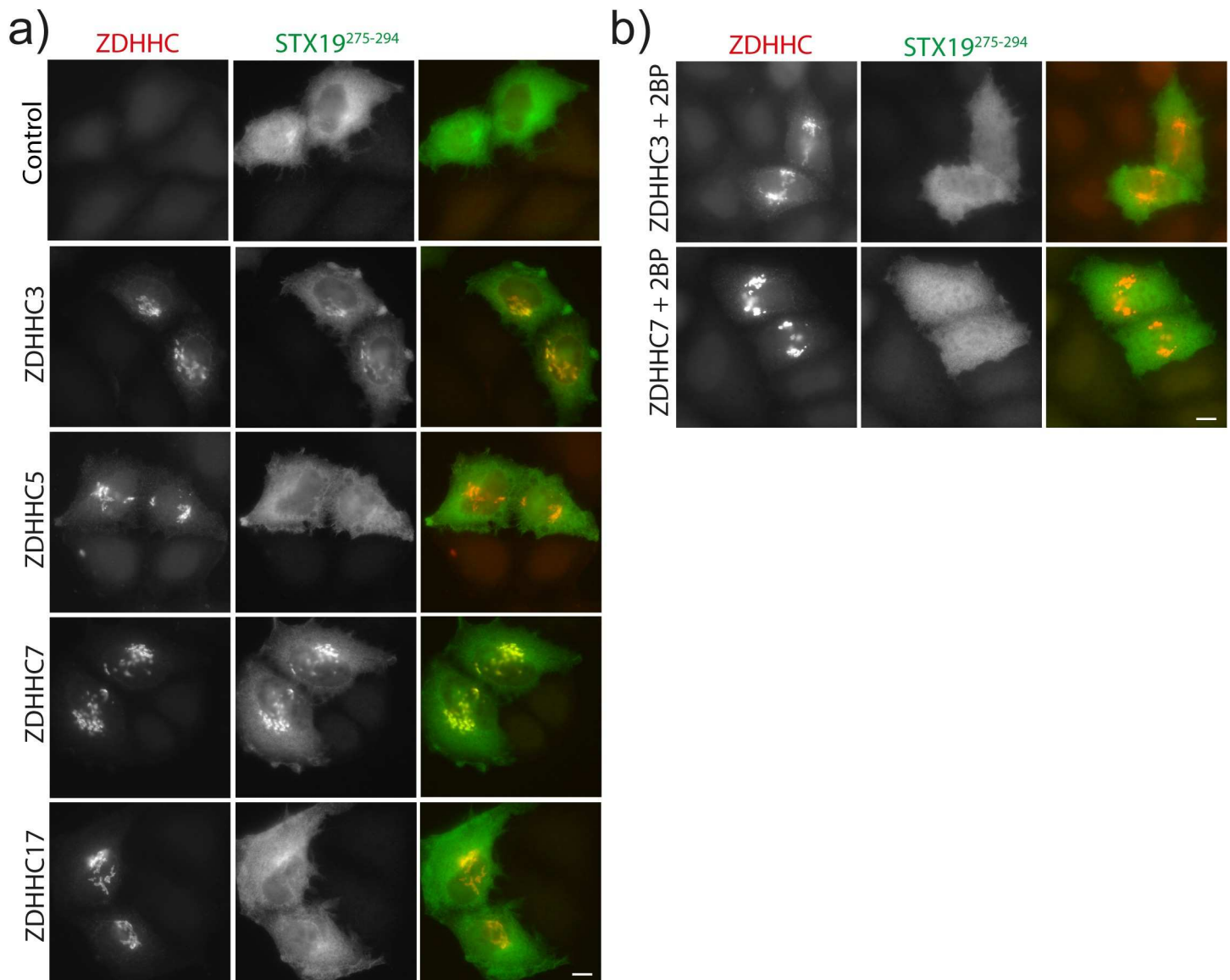
Fig S5. GFP-STX19²⁷⁵⁻²⁹⁴ can be S-acylated at the Golgi by zDHHCs 3 and 7.
A) HeLaM cells were grown on coverslips overnight and co-transfected with GFP-STX19²⁷⁵⁻²⁹⁴ and the indicated enzymes. The cells were fixed 6 hours post transfection and then stained with antibodies against HA and GFP. In the control cells, GFP-STX19²⁷⁵⁻²⁹⁴ is predominantly cytoplasmic while in the cells over expressing zDHHCs 3 or 7 it is localised to the Golgi. **B)** In a parallel experiment, cells transfected with zDHHCs 3 or 7 were also treated with 100 μM 2-BP. In the 2-BP treated cells the Golgi localisation is lost indicating that it is due to increased S-acylation of GFP-STX19²⁷⁵⁻²⁹⁴. Scale bar 10 μm.

Table S1. Representative protein sequences used to perform the sequence alignment shown in Fig. 2.

Species	C-terminal protein sequence
Homo sapiens	KYKKRNPCRVLCCWCCPCCSSK
Mus musculus	KYKKRNPCRALCCCCCPRCGSK
Canis lupus familiaris	KYKKRNPCKVLCCWCCPCCSSK
Equus ferus caballus	KYKKRNPCRVLCCWCCPCCGSK
Ornithorhynchus anatinus	RYKKRNPCRVLCCWCCSCCN
Gallus gallus	RYRKRHPCKVICCWCCPCCK
Ophiophagus hannah	KYRKKNPCKALCCWCCSCCK
Danio rerio	RYKKNNPLRRLCCCCCPWFR
Xenopus tropicalis	KYKRKNPCRALCCCCFPCCK

Table S2. Mass spectrometry data associated with S-acylation site identification in STX19. Peptide sequence information and identification scores (PEP) are provided for each S-acylated form. S-acylated residues are inferred by quantitative analysis of the relative levels of non-alkylated cysteine residues (i.e. protected from alkylation by S-acylation) +/- hydroxylamine treatment. Label free quantification of peptides +/- hydroxylamine treatment was performed using MaxQuant calculated peptide intensities in columns L-M for the STX19 tail construct (GFP-STX19 (275-294aa)) and in columns N-O for the full length STX19 construct (GFP-STX19 (1-294aa)).

Sequence	Mass adduct	Modification state	Mass	Proteins	Gene name	Charges	PEP	Score	Delta score	GFP-STX19 (275-294aa)		GFP-STX19 (1-294aa)	
										Intensity GFP-Stx19_Tail+HA	Intensity Stx19_Tail -HA	Intensity Stx19_FL +HA	Intensity Stx19_FL -HA
VLCCWCCPCCSSK	6 X Cys(+57 Da)	Unmodified	1775.638	Q8N4C7|STX19_HUMAN	STX19	2	7.26E-17	183.72	169.95	2.E+06	NaN	NaN	1.E+06
VLCCWCCPCCSSK	4 X Cys(+57 Da)	2 Palmitoylation	1661.595	Q8N4C7|STX19_HUMAN	STX19	2	5.44E-05	123.79	116.26	1.E+06	NaN	4.E+05	NaN
VLCCWCCPCCSSK	3 X Cys(+57 Da)	3 Palmitoylation	1604.574	Q8N4C7|STX19_HUMAN	STX19	2	0.031439	45.915	37.202	1.E+06	NaN	NaN	NaN
VLCCWCCPCCSSK	2 X Cys(+57 Da)	4 Palmitoylation	1547.552	Q8N4C7|STX19_HUMAN	STX19	2	0.006237	73.499	64.178	5.E+06	6.E+05	NaN	NaN
VLCCWCCPCCSSK	1 X Cys(+57 Da)	5 Palmitoylation	1490.531	Q8N4C7|STX19_HUMAN	STX19	2	0.002799	75.566	70.953	7.E+06	1.E+06	2.E+05	NaN
VLCCWCCPCCSSK	0 X Cys(+57 Da)	6 Palmitoylation	1433.509	Q8N4C7|STX19_HUMAN	STX19	2	0.00024	106.4	81.161	2.E+07	4.E+06	3.E+05	NaN